Interactions between turbidity currents and topography in aggrading sinuous submarine channels: A laboratory study

Kyle M. Straub[†][*]
David Mohrig[‡]
Brandon McElroy[‡]
James Buttles
Department of Earth, Atmosphere, and Planetary Sciences, Massachusetts Institute of Technology, 77 Massachusetts Avenue, Building 54-824, Cambridge, Massachusetts 02139, USA

Carlos Pirmez
Shell International Exploration and Production, Inc., P.O. Box 481, Houston, Texas 77001, USA

ABSTRACT

We present results from a laboratory experiment documenting the evolution of a sinuous channel form via sedimentation from 24 turbidity currents having constant initial conditions. The initial channel had a sinuosity of 1.32, a wavelength of 1.95, an amplitude of 0.39 m, and three bends. All currents had a densimetric Froude number of 0.53 and an initial height equal to the channel relief at the start of the experiment. Large superelevation of currents was observed at bend apexes. This superelevation was 85%–142% greater than the value predicted by a balance of centrifugal and pressure-gradient forces. An additional contribution to the superelevation was the runup of the current onto the outer banks of bends. This runup height is described by a balance between kinetic and potential energy. Runup resulted in deposition of coarse particles on levee crests that were indistinguishable from those deposited on the channel bottom. Deposit thickness and composition showed a strong cross-channel asymmetry. Thicker, coarser, steeper levees grew on the outer banks relative to the inner banks of bends. Zones of flow separation were observed downstream from bend apexes along inner banks and affected sedimentation patterns. Sedimentation from currents caused the channel to aggrade with almost no change in planform.

[†]E-mail: kmstraub@umn.edu
[*]Present address: St. Anthony Falls Laboratory, Department of Geology and Geophysics, University of Minnesota, Minneapolis, Minnesota 55414, USA
[‡]Present address: Department of Geological Sciences, University of Texas at Austin, Austin, Texas 78712, USA

However, channel relief decreased throughout the experiment because deposition on the channel bottom always exceeded deposition at levee crests. The first bend served as a filter for the properties of the channelized current, bringing discharge at the channel entrance into agreement with the channel cross-sectional area. Excess discharge exited the channel at this filtering bend and was lost to the overbank surface.

Keywords: turbidity current, leveed channels, sinuous channels, turbidite, superelevation.

INTRODUCTION

Channels are the most significant morphologic feature of the submarine landscape on the continental slope. Many of these channels are highly sinuous in planform (sinuosity, $s \geq 1.3$) and persist from 10 to 1000 km downslope, yet the processes by which these channels evolve and organize themselves are incompletely known. There are still very few direct observations of turbidity currents moving through sinuous channels (Hay, 1987; Khripounoff et al., 2003; Xu et al., 2004) because infrequent occurrence, great water depths, and high current velocities make measurements difficult to obtain. This paper presents results from a laboratory experiment where the interactions of currents with channel bends are directly monitored at a reduced scale. We focused on resolving processes controlling the construction of channel-margin levees and the nearly vertical aggradation of a channel with almost no change in its planform. This style of geometric and kinematic evolution is reported for many natural channels based on seismic imaging and analysis (Deptuck et al., 2003; Posamentier, 2003), and is a key component in a number of conceptual models for submarine channel evolution, including those by Peakall et al. (2000), Kneller (2003), and Pirmez and Imran (2003). It is the style of channel evolution most closely linked to a significant addition of sediment mass to the submarine landscape.

The nearly vertical climb of channel forms in space through time requires rates of overbank sedimentation that are comparable to those within the channels. The most commonly cited processes by which sediment is transferred from channelized turbidity currents to overbank flow are referred to as flow splitting and flow spilling (Clark and Pickering, 1996; Kassem and Imran, 2005; Peakall et al., 2000; Piper and Normark, 1983). Flow splitting describes a process where the upper fraction of the flow traveling above the channel detaches from the body of the current as it moves through a channel bend. This detachment takes place along the outer bank of a bend, and afterward the separated fraction of current is thought to move independently out across the overbank surface (Piper and Normark, 1983). Flow spilling, however, is not a site-specific mechanism. Flow spilling describes a process in which a suprachannel fraction of a current spreads laterally out across the overbank surface (Clark and Pickering, 1996). This lateral spreading primarily is interpreted as being a consequence of the gravitational collapse of the non-confined portion of the density current. Another recognized process that produces overbanking flow was referred to as inertial overspill by Hay (1987). Inertial overspill of currents at bends is a result of spatial changes in channel width and takes place only when curvature of an outer bank exceeds that of the channel axis. The experiment presented here specifically investigates the

consequences of the more general flow splitting and overspilling on construction of the overbank surface and channel-bounding levees. Recent conceptual models that describe the long-profile evolution of a current call on a systematic bias in the size of suspended particles that leave a channel. The effect is a coarsening in the particle-size distribution for the remaining channelized current with distance traveled (Peakall et al., 2000; Posamentier and Kolla, 2003). These conceptual models remain untested for natural systems but are tested here at laboratory scale.

Laboratory models exploring phenomena of landscape-evolving flows at reduced scale must resolve three separate but coupled fields in order to be complete: (1) the topography and composition of the evolving granular bed; (2) the sediment transport field; and (3) the flow field. In practice, even under controlled laboratory conditions, it is difficult to monitor the structure and evolution of all three fields equally well. Typically attention is focused on one or two of the fields at the expense of the others, depending on the guiding motivation for the study. The experiment presented here focuses on evolution of the channel form and the composition of the sedimentary deposits that modify its topography. Measurements defining the other two fields were also collected but emphasis was placed on resolving the geometric and kinematic evolution of the vertically aggrading channel. We made this choice in order to generate data that are consistent with the greatest amount of information available for natural submarine channels, seismic images of their topography, and their affiliated deposits.

Recent laboratory measurements reported by Imran et al. (2007), Corney et al. (2006), and Keevil et al. (2006), and numerical models of Imran et al. (1999), Kassem and Imran (2005), and Corney et al. (2006) provided quantitative descriptions or estimations of the flow fields associated with gravity currents traversing a series of sinuous channel bends. The laboratory measurements in particular make important contributions to defining both the structure of the mean flow and the turbulence intensities associated with these gravity currents. While this information is critical to developing a general understanding of the fluid dynamics, the absence of sediment transport and/or deposition in these studies prohibits direct observation of the coevolution of turbidity currents and the channels they construct. Measurements of this coevolution, connected through the sediment transport, are a necessary component for models of submarine landscape evolution. We present results from an experiment where strongly depositional currents modified a preexisting channel by spatially varying patterns of sedimentation. These measurements are intended to

serve as a benchmark for developing and calibrating fully three-dimensional (3-D) numerical models of flow through sinuous submarine channels. At the present time, numerical models describing channelized 3-D turbidity currents either assume that the currents are completely confined to the channel (Das et al., 2004; Imran et al., 1999) or that they are conservative and therefore unable to evolve the channel form (Imran et al., 2002; Kassem and Imran, 2005). The experiment presented here targets a middle ground between these end-member configurations in an attempt to capture the interactions between currents and topography most relevant to building depositional channel forms.

Due to a lack of direct measurements of the interactions of currents with submarine channels, many scientists have focused on reconstructing flow conditions by interpreting depositional and erosional patterns preserved in seafloor topography and in sedimentary deposits (Bouma, 2000; Gardner et al., 2003; Komar, 1969; Lee et al., 2002; Middleton, 1993; Pirmez, 1994; Pirmez et al., 2000; Pirmez and Imran, 2003; Shor et al., 1990). Models developed for subaerial channelized flow have been applied as semiquantitative guides for understanding the physics of flow through sinuous submarine channels (Imran et al., 1999; Komar, 1969; Pirmez and Imran, 2003). For example, Komar (1969) estimated a mean streamwise velocity for turbidity currents that moved through the Monterey Canyon by assuming that the unequal heights of levees extending along the outer and inner banks of channel bends recorded a cross-channel superelevation of currents that was set by the balance between centrifugal and pressure-gradient forces. Use of the terrestrial analog has been considered reasonable because rivers and submarine channels have been found to share the same scaling relationships between meander wavelength, radius of curvature, and bend amplitude (Clark et al., 1992; Hay et al., 1983; Leopold and Wolman, 1960; Pirmez, 1994). While the similarities in geometry between channels of the two environments do exist, both computational (Corney et al., 2006; Kassem and Imran, 2005) and experimental (Imran et al., 2007; Keevil et al., 2006) analyses point to key differences between the flow fields of terrestrial versus submarine sinuous channels. One consequence of these differences is the relatively high rate of overbank sedimentation in the submarine environment allowing nearly vertical climb of submarine channel forms (Hackbarth and Shew, 1994; Kneller, 2003; Peakall et al., 2000; Posamentier et al., 2000; Stelting et al., 1985). High rates of overbank sedimentation are most pronounced along the outer banks of channel bends in the submarine where thick

channel levees are deposited (Hay, 1987; Pirmez and Flood, 1995; Posamentier and Kolla, 2003; Prior et al., 1987). We are interested in determining which processes account for this apparent increase in overbank sedimentation. In this sense, our laboratory results can be used to examine differences between subaerial and subaqueous flows moving through sinuous channels and provide an opportunity to better understand channelized landscapes in general.

EXPERIMENTAL SETUP

We released 24 sediment-laden currents into a basin that is 5 m long, 5 m wide, and 1.2 m deep, that remained filled with water throughout the experiment (Fig. 1). Before filling the basin with water, a channel was built on its floor with a sinuosity of 1.32 and a planform described by a sine-generated curve that has been shown to reproduce the shape of many subaerial and subaqueous channels (Langbein and Leopold, 1966; Pirmez, 1994). This curve describes the local direction of the channel centerline, φ, as a function of streamwise distance, x:

$$\varphi = \omega \sin \frac{x}{X_t} 2\pi , \qquad (1)$$

where ω is the maximum angle at which the centerline deviates from the mean downstream direction and X_t is the centerline distance associated with one channel wavelength. Our channel was designed with $\omega = 55°$, $X_t = 3.4$ m, and a bend wavelength and amplitude of 1.95 m and 0.39 m, respectively. Channel sidewalls and banks were constructed from a 15:1 mixture of sand and cement mortar. The original channel was trapezoidal in cross section with an initial depth of 0.11 m and basal and top widths of 0.20 m and 0.40 m, respectively (Fig. 1). The channel was built with no downstream bed slope. After traversing the 4.2-m-long channel, each current spread out onto a short unconfined surface before plunging into a moat where it was removed from the basin via perforated pipes, thereby preventing current reflections off of the tank sidewalls.

All turbidity currents were composed of the same mixture of clear water, dissolved $CaCl_2$, and suspended sediment. This mixture produced currents that entered the channel with an absolute density of 1021 kg/m³ and an excess density of 2.1% relative to the fresh water that filled the basin. Of this excess density, 33% was due to suspended sediment and 67% was from the dissolved salt. The sediment consisted of 60% blown silica (ballotini) and 40% crushed silica flour by weight with a cumulative size distribution, where $D1$, $D5$, $D10$, $D16$, $D25$, $D50$, $D75$, $D84$, $D90$, $D95$, and $D99$ equaled nominal diameters of 1.7 μm, 3.1 μm, 12.9 μm,

18 μm, 23 μm, 31 μm, 41 μm, 46 μm, 52.1 μm, 60 μm, and 80 μm, respectively (Fig. 2). Dissolved salt was used to simulate the finest portion of suspended sediment within natural turbidity currents, a fraction that is transported to the distal end of a system without loss via deposition. The mixture of water, sediment, and dissolved salt was introduced to the basin via a constant head tank that guaranteed steady input discharge throughout each individual release. Each current passed through a momentum extraction box before entering the channel. This box was 0.5 m by 0.5 m in planform and contained several vertical screens of 5-mm wire mesh through which currents passed prior to entering the experimental channel. The momentum extraction box ensured that each flow acted as a sediment-laden plume driven by buoyancy alone. Current thickness and discharge at the channel entrance were held constant for all 24 runs at values of 0.11 m and 4.7×10^{-3} m³/s. Representative input values for the densimetric Froude number

$$\left\{ Fr = \bar{u} \, / \, \sqrt{\left[(\rho_c / \rho_a) - 1 \right] gH} \right\},$$

Reynolds number $\left(Re = \bar{u}H / \upsilon \right)$, and buoyancy flux $\left(B_{f0} = \Delta\rho g u H b / \rho \right)$ were 0.53, 8.2 × 10³ and 5.3×10^{-4} m⁴/s³, respectively, where $\bar{u}$ is depth-averaged velocity, ρ_c is current density, ρ_a is the ambient fluid density, g is gravitational acceleration, H is current thickness, υ is kinematic viscosity, and b is mean channel width. The duration of each current was 5.3 ± 0.1 min. The flow of currents out of the momentum extraction box and into the experimental channel represents a similar transition made by erosional currents confined in canyons to depositional currents in aggradational channels.

Measurements of current velocity were collected using two Sontek acoustic Doppler velocimeters (ADV) and one Sontek pulse-coherent acoustic-Doppler velocity profiler (PCADP). An ADV was positioned at the channel entrance and exit throughout the experiment. These devices recorded the 3-D velocity in a 2×10^{-7} m³ sampling volume located 50 mm above the channel bed at the channel centerline with a frequency of 10 Hz. Vertical profiles of velocity were measured at many locations inside and outside of the channel using only one of the three transducers on the PCADP. The PCADP measured velocity with a frequency of 0.25 Hz in roughly cylindrical sampling volumes that were 1.6×10^{-2} m deep and had a horizontal footprint that varied in diameter from 7.1×10^{-2} m to 8.7×10^{-2} m with increasing distance from the transducer. Key PCADP sampling locations were the proximal overbank surface at the apexes of bends 1 and 3, as well as at the bed of the channel, the inflection points between the three bends. Repeated
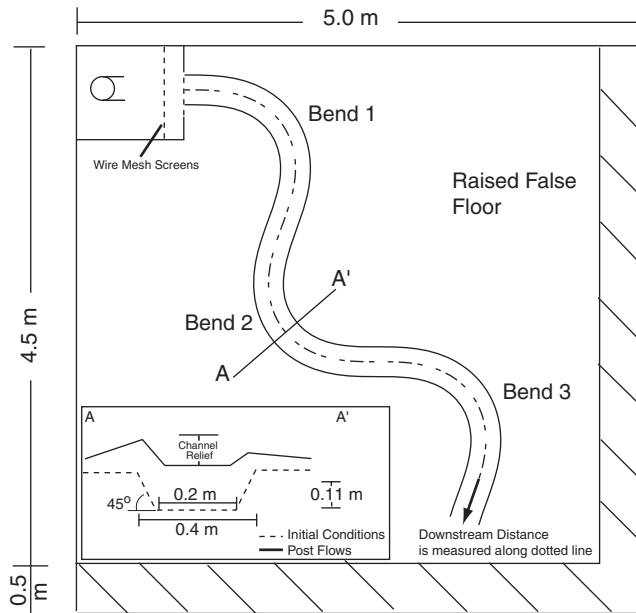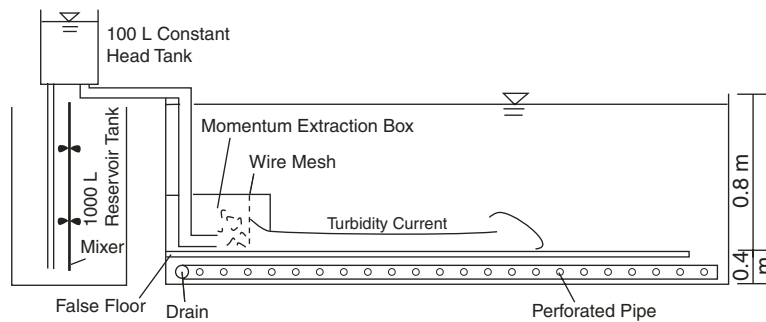

Figure 1. Schematic diagram of the experimental facility. (A) Plan view of the basin and the initial channel form. Each current passed through a momentum extraction box located in the top left basin corner prior to entering the channel. Diagonal lines mark the position of a moat for collecting a current following its passage through the channel, avoiding reflections off of tank walls. The inset depicts an initial and final channel cross section. (B) Side view of the facility. Each current is mixed in a reservoir tank and pumped up into a constant head tank before entering the basin.
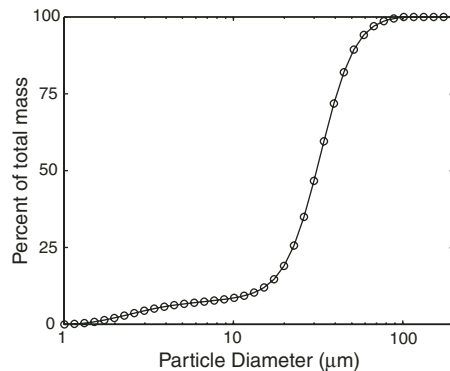
Figure 2. Particle size distribution for sediment discharged into experimental basin.
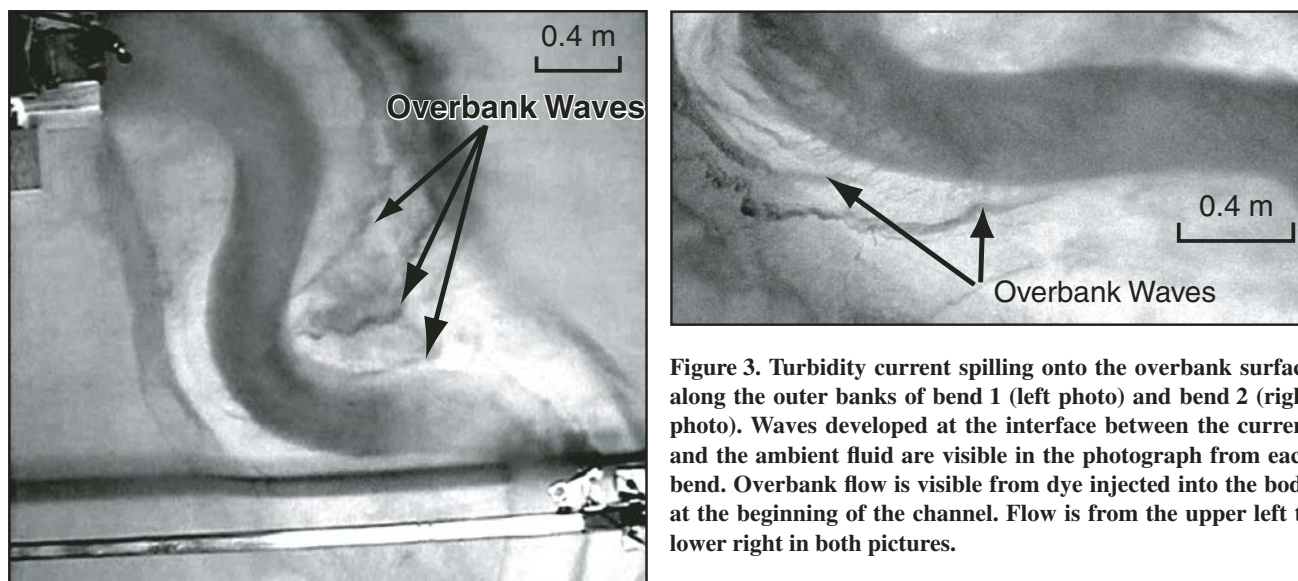
Figure 3. Turbidity current spilling onto the overbank surface along the outer banks of bend 1 (left photo) and bend 2 (right photo). Waves developed at the interface between the current and the ambient fluid are visible in the photograph from each bend. Overbank flow is visible from dye injected into the body at the beginning of the channel. Flow is from the upper left to lower right in both pictures.

measurements at these points assured the capture of any changes in velocity and thickness of the currents as the channel-form evolved.

Aerial video was collected throughout the duration of each current. These overhead videos recorded passage of the head of the current through all three bends, as well as its movement out onto the overbank surface. The overall structure of the flow field associated with the body of each current was imaged by releasing a 15 mL pulse of dye at the channel entrance ~2 min following the start of each flow. These dye pulses were captured on the overhead video, and the mapping of dye-front positions through time was used to define the magnitude and direction of the local maximum horizontal velocity throughout the coupled channel-overbank flow field (Fig. 3 and GSA Data Repository Fig. DR1[1]). The PCADP transducer when positioned on the overbank surface at outer banks of bends 1, 2, and 3 was oriented so that it collected velocity data in the direction of maximum horizontal overbank velocity as clearly defined by dye-pulse measurements. The structure of the suspended-sediment profile, i.e., sediment concentration and grain size, was measured via a rack of vertically stacked siphons positioned at the channel centerline at the points of inflection between bends 1 and 2 and 2 and 3.

Maps of the channel form following each experimental current were produced using the first hard returns from a 1-MHz ultrasonic transducer connected to a pulse-receiver box. Each

bathymetric map was built from 27,600 points collected on a grid with 5 mm spacing in the cross-stream direction and 40 mm spacing in the downstream direction. The precision at each location is better than 0.2 mm. This resolution makes it possible to successfully determine the patterns of sediment deposition associated with individual currents by differencing successive maps of channel topography.

Following the 24th current, the water level in the experimental basin was lowered, and the deposit was allowed to dry. After drying, the deposit was sampled for particle-size characterization. These samples were collected at 211 locations along 13 channel cross sections oriented perpendicular to the channel centerline. At most of these locations, the deposit was divided into lower, middle, and upper samples. The sediment samples were then analyzed with a Horiba LA-300 laser-particle-size analyzer (LPSA). The LPSA uses a diode laser to accurately measure a distribution of sizes from 0.001 to 0.3 mm in nominal diameter.

Scaling

Our experiment was conducted at a reduced scale relative to submarine channels. It is therefore important to discuss how our model system compares to the natural environment. This comparison has three components: (1) a simple geometric scaling of the relatively static channel topography; (2) a dynamic scaling of flow properties for estimating equivalence between model and natural flows; and (3) a dynamic scaling of the sediment transport in order to roughly compare particle sizes being moved by the model and natural flows. The scaling is only intended to guide how experimental

results might be applied to the interpretation of natural channels. Our experiment was not designed to simulate environmental conditions associated with a specific system, but rather was carried out to better understand the depositional consequences of interactions between turbidity currents and channels.

The geometric scaling for our experiment was chosen to be 1/1000. Maximum width, depth, and length for the laboratory channel therefore correspond to natural scales of 400 m, 110 m, and 3.5 km. Bend amplitude and wavelength correspond to natural scales of 390 m and 1.95 km. The wavelength/amplitude ratio was 6.5 and the channel width/depth ratio measured at the inflection point between bend apex 1 and 2 systematically increased from 3.6 to 8.0 through the course of the experiment. These values compare favorably with measurements from natural channels assembled by Pirmez and Imran (2003): wavelength/amplitude ranges between 0.4 and 8.0, and values of width/depth for the Amazon submarine channel tightly cluster around 10. A comparison of our channel geometry to the Amazon submarine system and recent numerical and experimental studies is found in Table 1.

The comparison between properties of the experimental and natural or prototype flows focuses on the densimetric Froude number. An approximate dynamic similarity between the model and a natural system is ensured by setting $Fr_{(model)} = Fr_{(prototype)}$ (Graf, 1971). Assuming a similar excess density for the experimental and natural currents, equality in densimetric Froude number is satisfied by prototype values for $\bar{u}$ and H of 2.5 m/s and 110 m (Table 2). Equality in densimetric Froude number also constrains the duration of a comparable natural current (T) to

---

TABLE 1. COMPARISON OF OUR EXPERIMENTAL CHANNEL AND CURRENTS
TO THEORETICAL AND LABORATORY STUDIES

	Kassem and Imran (2005)	Das et. al. (2004)	Keevil et al. (2006)	This study	Amazon[a,b]
	1.13	1.3	1.36	1.32	1.2–2.6
λ/W	10	9.4	5.09	5	3–7
λ/r_0	4.4	7.8	3.1	3.3	3–6
r_0/W	2.3	1.6	1.6	1.5	1–1.5
W/D	=<10.6*	5.5	1.8	3.6–8.0	9–25
Downstream slope	$0.08°$	$0.3°$	$3°$	$0–1.20°$	$0.14–0.40°$
Sidewall slope	$90°$	$90°$	$79°$	$21–45°$	$15–25°$
Froude Number	1.22	1.46	0.63	0.53	0.5–0.8

*Currents were completely confined to channel; [a]Pirmez and Flood (1995); [b]Pirmez et al. (2003).
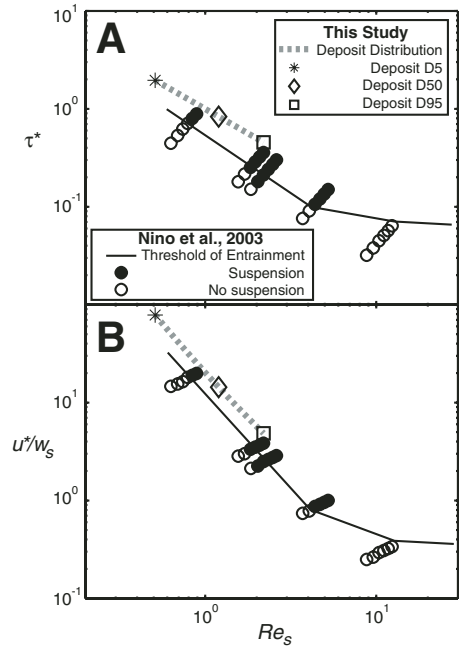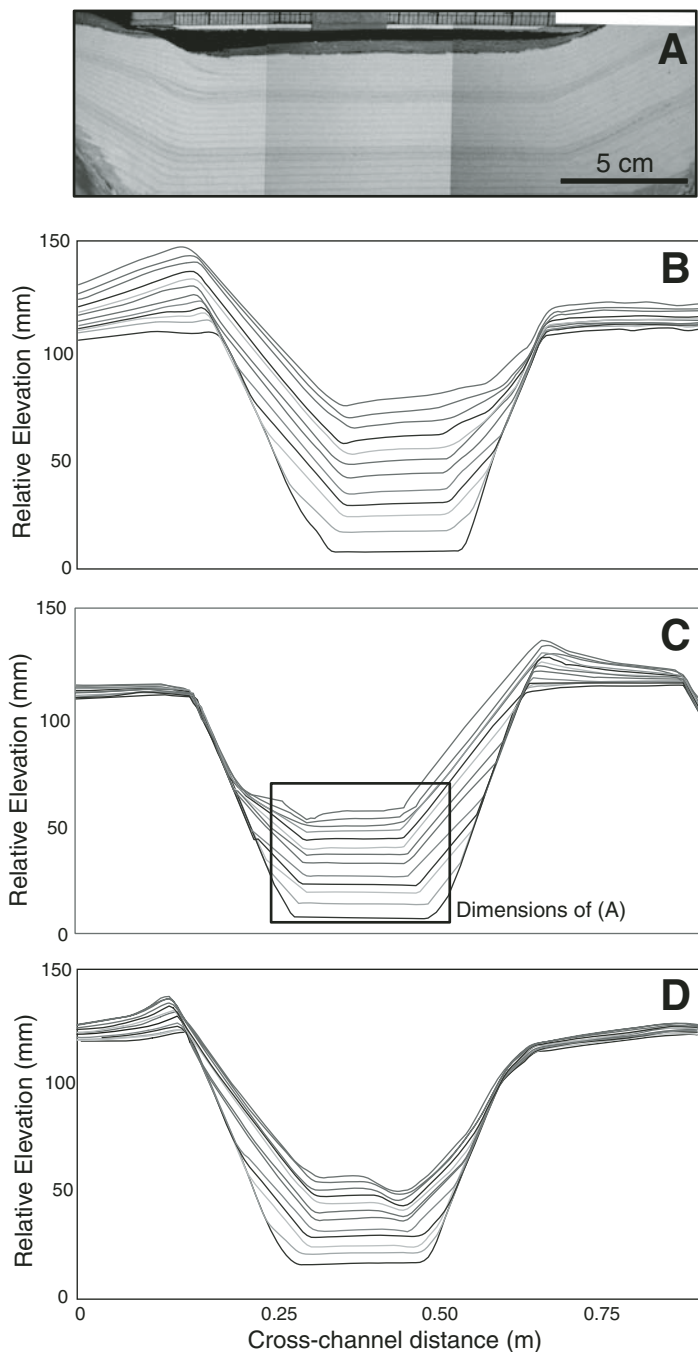*Note*: r_0—channel centerline radius of curvature; D—particle diameter.

Figure 4. Comparison of experimental conditions in this study to threshold of particle entrainment into suspension conditions reported by Nino et al. (2003). Circles represent measurements of Nino et al. (2003) and black solid lines are proposed threshold conditions. Gray dashed line represents experimental conditions in this study defined between diameter (D), $D5$ and $D95$ particle sizes of deposit at channel axis at apex of bend 2. (A) Threshold of particle entrainment into suspension defined by Re_s and τ^*. (B) Threshold of particle entrainment into suspension defined by Re_s and u^*/w_s.

be 2.7 h. Reynolds numbers for the model and prototype cannot be matched. The characteristic Reynolds number for model currents was 8.2×10^3 while the characteristic value for a comparable natural current would be 3.0×10^8. Fortunately the model-current value was sufficiently large to ensure the approximate Reynolds similarity for fully turbulent gravity currents proposed by Parsons and García (1998).

Altinakar et al. (1996) showed that the lower portions of velocity profiles for turbidity currents developing on a flat bed under approximately steady and uniform conditions exhibit a logarithmic form that can be described by

$$u(z) = \frac{u^*}{\kappa} \ln\left(\frac{z}{z_0}\right), \qquad (2)$$

where $u(z)$ is the time-averaged streamwise velocity as a function of elevation above the bed, z, κ is von Kármán's constant and is equal to 0.4, and z_0 is a roughness parameter, equal to the elevation at which the extrapolated logarithmic velocity profile goes to zero. We have estimated the characteristic shear velocity associated with the model currents, u^*_{model}, by fitting equation 2 to velocity data collected with the PCADP from 8 of the 24 experimental currents. The fit to the portion of the velocity profiles situated between and bed and the velocity maximum is good, with the average R^2 = 0.91 (Fig. DR2; see footnote 1) and u^*_{model} = $2.5 \pm 0.7 \times 10^{-2}$ m/s. A characteristic friction coefficient, C_f, for the model currents can be

calculated from this estimate for u^*_{model} and the measured $\bar{u}_{model} = 8.0 \times 10^{-2}$ m/s using

$$u^* = \sqrt{C_f \bar{u}} . \qquad (3)$$

The resulting $C_{f(model)} = 9.8 \times 10^{-2}$ is consistent with other laboratory measures of $C_{f(model)}$ for turbidity currents reported by Parker et al. (1987) and Garcia (1994). A prototype shear velocity can be determined using equation 3 and the estimated values for $\bar{u}_{prototype}$ and $C_{f(prototype)}$ of 2.5 m/s and 9.8×10^{-3}. We have reduced the prototype value for C_f by an order of magnitude to account for the weak dependence of bed friction coefficient with turbidity-current scale as summarized in Parker et al. (1987) and Garcia (1994). The calculated $u^*_{prototype} = 2.5 \times 10^{-1}$ m/s.

Grain sizes used in the experiment can be compared to natural channels by estimating equivalent sediment transporting conditions between the two systems. Since the predominant mode of transport is suspended load, we make the dynamic comparison by matching the ratio w_s/u^*. This scaling parameter was chosen because it best characterizes the degree to which particles of various sizes are suspended within the transporting current, with w_s serving as the scale value for downward particle advection and u^* being the scale value for the effective diffusion of particles into the interior flow by turbulent eddies. Particle settling velocities for $D5$, $D10$, $D50$, $D90$, and $D95$ were 5.1×10^{-5} m/s, 1.3×10^{-4} m/s, 7.8×10^{-4} m/s, 2.0×10^{-3} m/s, and 2.7×10^{-3} m/s, respectively. Calculated experimental values for $w_s/u^*_{(D5)}$, $w_s/u^*_{(D10)}$, $w_s/u^*_{(D50)}$, $w_s/u^*_{(D90)}$, and $w_s/u^*_{(D95)}$ are 2.0×10^{-4}, 5.0×10^{-3}, 3.1×10^{-2}, 8.4×10^{-2}, and 1.1×10^{-1}. All five of these values are much less than 1, the minimum value for significant suspension transport originally reported by Bagnold (1966). By satisfying the equality $w_s/u^*_{(model)} = w_s/u^*_{(prototype)}$, we estimate that $D5$, $D10$, $D50$, $D90$, and $D95$ for the experimental flows correspond to particle sizes of 8 µm, 40 µm, 110 µm, 210 µm, and 251 µm for flows at natural scale.

The above sediment-transport scaling is directed at estimating properties associated with the interiors of currents. We are also interested in

TABLE 2. COMPARISION OF MODEL AND
PROTOTYPE FLOW CHARACTERISTICS

	Model	Prototype
$\bar{u}$ (m/s)	0.08	2.5
H (m)	0.12	120
T (hr)	8.8×10^{-2}	2.7
Fr	0.53	0.53
Re	8.2×10^3	3×10^8
C_f	3×10^{-2}	3×10^{-3}
u^* (m/s)	0.014	0.14
$w_{s(D50)}$ (m/s)	7.8×10^{-4}	8.1×10^{-3}
$w_{s(D50)}/u^*$	5.6×10^{-2}	5.6×10^{-2}
$D50$ (µm)	31	113

assessing near-bed conditions using the particle Reynolds number, $Re_s = u^*D/\upsilon$. The appropriate model and prototype values for u^* and $D95$, as well as $\upsilon = 9.8 \times 10^{-7}$ m²/s, yield estimates for $Re_{s(model)}$ and $Re_{s(prototype)}$ of 2.0 and 42. For the case of a flat bed the experimental system has a hydraulically smooth boundary and the natural system has a hydraulically transitional boundary, implying that scale of particles composing the beds is smaller than (model) or comparable to (prototype) the thickness of the viscous sublayer (Graf, 1971). In both cases viscous effects are important in setting the style of the near-bed sediment-transport conditions. Nino et al. (2003) performed a set of experiments to determine threshold conditions for the entrainment of bed sediment into suspension for cases of small Re_s where viscous effects are significant. These threshold conditions for particle entrainment into suspension are plotted in Figure 4 as functions of Re_s, u^*/w_s, and dimensionless bed

Figure 5. Photograph of sectioned deposit at 2nd bend apex (A). Evolution of channel cross sections located at the apexes of the first (B), second (C), and third (D) bends. Each figure displays the original channel form plus successive forms following sedimentation by two currents. All cross sections are oriented perpendicular to the local centerline direction and oriented looking downstream.

shear stress [$\tau^* = u^{*2}/(RgD)$], where R is the submerged specific density for particles of representative diameter D. Estimated values for Re_s, u^*/w_s, and τ^* for our experiment are also plotted in Figure 4. These values indicate that experimental conditions associated with our model are within the suspension regime as measured and predicted by Nino et al. (2003).

EXPERIMENTAL RESULTS

The primary goal of this experiment was to characterize the patterns in sediment deposition associated with turbidity currents moving through a sinuous channel. We were particularly interested in determining how channel curvature, distance from the source, and the relative thickness of currents controlled the patterns of deposit thickness and grain-size composition, both inside and outside of the channel. A representative cross-sectional view of the 24 deposits that aggraded the channel bottom is shown in Figure 5A. Sectioning the deposit revealed that each flow laid down a sediment lamina with no observable internal structure and a fine-grained cap consisting of particles that did not settle out from the water column until after each current was finished. Preservation of these sub-millimeter-thick caps documents that there was almost no reworking of particulate bed material by subsequent currents and highlights the constructional character of the evolving channel form and its affiliated deposit. The surface of the deposit primarily was smooth with local development of ripples. Between the apexes of bend 1 and bend 3, ripples were observed on the levee bounding the outer margin of bend 1 and locally in the channel thalweg at bends 2 and 3. From overhead photographs of the channel following current 24 we estimate that 5% of the channel bed between bends 1 and 3 was worked into ripple forms. Ripple heights, wavelengths, translation distances, and climb angles were measured at the apex of bend 2 from vertical sections cut through the deposit in the streamwise direction following completion of the experiment. These sections revealed stratification produced by a supercritical angle of ripple climb (Rubin and Hunter, 1982). Ripple translation distances associated with each current were straightforward to measure because the complete ripple forms were preserved from current to current. These distances were converted to minimum translation rates by assuming that where present, ripple movement occurred throughout the duration of each current. The resulting estimate for mean translation rate together with measures for mean ripple height and length and a value for bed porosity of 0.35 were used to estimate a bedload transport rate following the method of

Simons et al. (1965). Applying this local value to the 5% of channel-bed area worked into bedforms yields a downstream bedload transport rate for the channel section of $2 \pm 1 \times 10^{-10}$ m^3/s. This estimate for bedload transport rate is very small relative to the channelized suspended sediment flux measured using a rake of siphons positioned at the inflection point on channel centerline between bends 2 and 3. The resulting estimated rate for downstream suspended-sediment transport was $8 \pm 2 \times 10^{-6}$ m^3/s. This estimate of suspended sediment load flux is 40,000 times greater than our estimate of bedload flux using the preserved ripples. We think that this result serves as independent confirmation for the previously developed estimate following the methods of Nino et al. (2003) that near-bed sediment transport in the experimental channel was dominated by grain suspension.

The predominance of structureless, channel-mantling lamina (Fig. 5A) and the supercritical angle of ripple climb point to sedimentation patterns that were primarily associated with the rain of suspended sediment onto the bed. The only evidence for reworking of bed material by bedload processes are the aerially restricted trains of ripple forms, and analysis of a representative deposit at bend 2 showed how little these structures modified the deposit. Individual ripples were observed to migrate $<1 \times 10^{-2}$ m during any single current, and climbing at a supercritical angle ensured very little reworking of the accumulating deposit by subsequent ripple migration (Rubin and Hunter, 1982). Patterns of lamina thickness and grain size are therefore interpreted as preserving properties of sediment deposition from suspension with minimal modification by bedload processes. These laminae represented the solids lost from each current during its traverse of the channel segment, and this sediment volume was small when compared to the total amount carried by a current. The deposited fraction was very close to 10% for the early currents and had increased to 15% by current 24. A majority of the sediment bypassed the mapped region, exiting the channel at its downstream end. Evolution of channel topography associated with this limited amount of sediment deposition on the channel bed, sidewalls, and banks is described below.

Deposition on Channel Bed and Sidewalls

Each turbidity current produced a deposit that systematically decreased in thickness and grain size with distance down the channel centerline (Figs. 6, 7A, and 8). The stacking of tapered deposits generated a centerline bed slope that increased in magnitude throughout the experiment. At the beginning of the
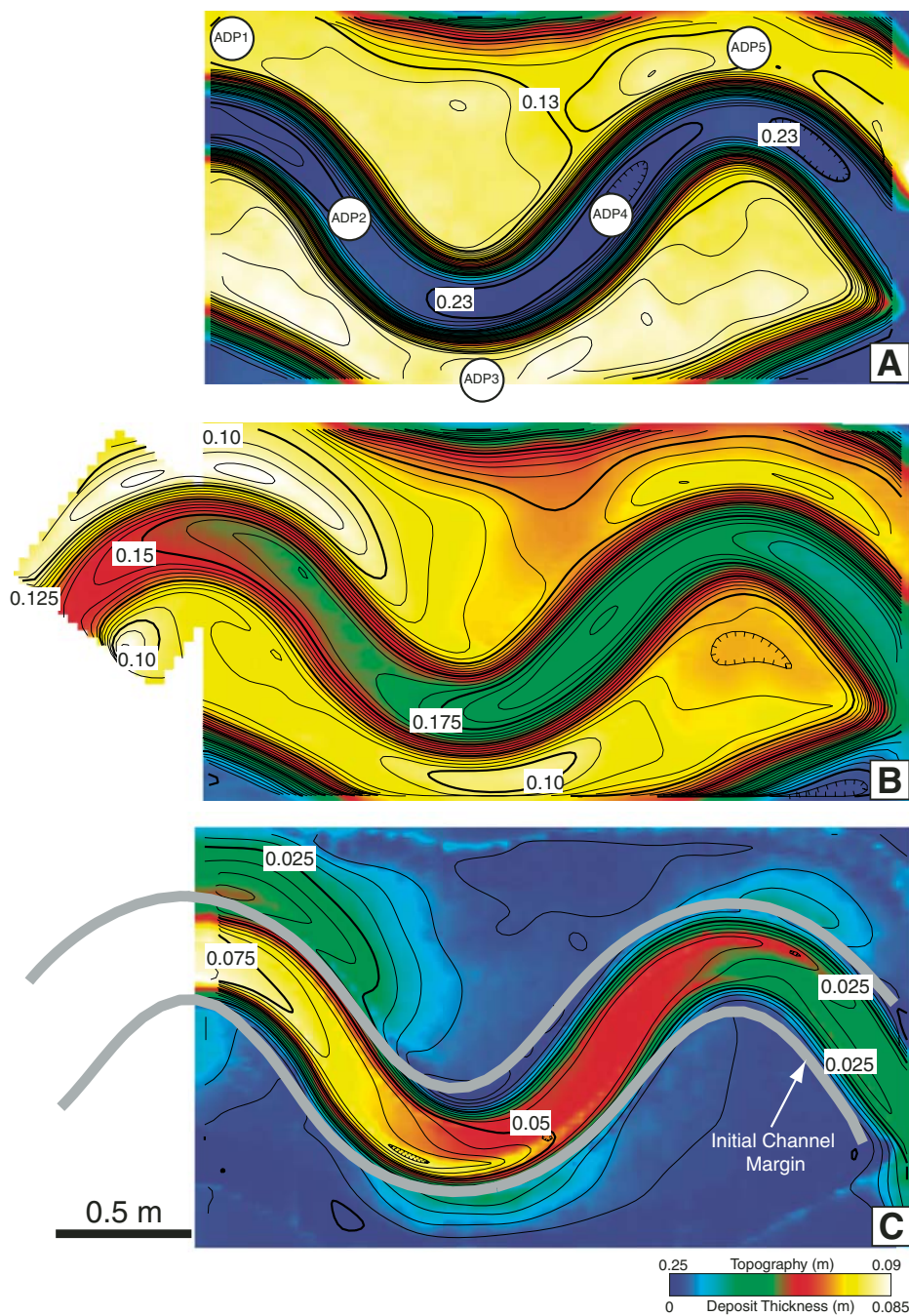
Figure 6. Maps from the experimental channel. Channel flow was from the left to the right in each map. (A) Topographic map of the initial channel form. Topography is defined as vertical distance between the bed and an overlying datum of constant elevation. Contour interval is 5 mm. Locations of pulse-coherent acoustic-Doppler velocity profiler (PCADP) measurements discussed in text are marked in the map. Velocity profiles collected at the ADP2 and ADP3 locations were used to constrain current superelevation at bend 2, and profiles at ADP4 and ADP5 were used to constrain superelevation at bend 3. (B) Topographic map of the final channel form following sedimentation by 24 currents. Channel filling and pronounced levee growth along the outer banks of the three bends are clearly defined. Contour interval is 5 mm. (C) Map of deposit thickness from sedimentation by 24 turbidity currents. This map is the difference between maps A and B. Contour interval is 5 mm. Gray bold lines represent location of channel margin prior to deposition by flow 1.
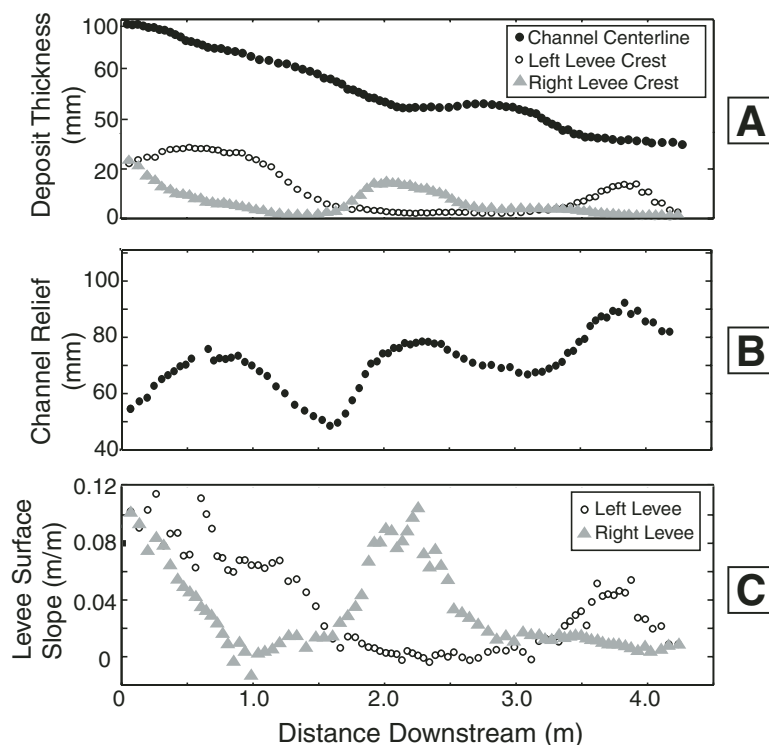
Figure 7. Downstream trends following sedimentation by 24 currents. (A) Deposit thickness as a function of distance along the channel centerline. Levee-crest deposits were measured on cross sections oriented perpendicular to the local direction of the channel centerline. Left and right levee refer to the left and right margins of the channel when looking downstream. (B) Channel relief as a function of distance along the channel centerline. Relief was measured using channel cross sections cut at right angles to the local centerline direction and equaled the elevation difference between the channel bed at the centerline and the taller of the two levee crests on that particular cross section. (C) Levee surface slopes as a function of distance along the channel centerline. Surface slopes were measured on channel cross sections cut orthogonal to the local centerline direction.

Deposition on Channel Banks

Deposition on the overbank surface displayed down-system trends that were roughly similar to those already described within the channel; thickness of the deposit and grain size decreased with distance from the channel entrance. Superimposed on these trends was a pronounced asymmetry in deposit properties that varied with local curvature of the channel. The outer banks of all three bends were sites of pronounced levee construction (Fig. 5). These wedge-like overbank deposits were not evenly distributed about the bend apex (Fig. 6). Position of the thickest levee deposit at the 1st, 2nd, and 3rd bend was displaced downstream from the point of maximum channel curvature by distances of 0.12 m, 0.10 m, and 0.12 m, respectively (Fig. 6). Overbank deposits that accumulated directly across the channel on the inner banks of bends were, in general, thinner, finer grained, and less wedge-like in cross section (Fig. 5). Specific measurements defining the differences in overbank sedimentation between outer and inner banks of bends are presented below.

Surface slopes of the constructional overbank surface varied with the local channel curvature. Values of this slope were measured at the end of the experiment along transects running perpendicular to the local centerline direction. These transects revealed that levees forming along the outer banks of bends have higher slopes than those developed along the inner banks (Fig. 7C). The maximum surface slope for outer-bank levees at bends 1, 2, and 3 were 0.10, 0.12, and 0.06, respectively. The maximum slope measured for the affiliated inner-bank levees at bends 1, 2, and 3 were 0.06, 0.01, and −0.04, respectively.

The measured surface slopes provide a reasonably accurate estimate of the wedge-like geometry associated with the overbank deposits because they accumulated on an original surface that was close to horizontal. This is not often the case for natural surfaces, making levee taper a superior measure of cross-sectional form. We define levee taper as the change in deposit thickness over a specified distance extending perpendicular to the local direction of the channel centerline. Tapers for outer-bank levees are calculated using the deposit thicknesses at levee crests and at positions located 0.15 m outboard from the crests. These measures defined the spatial rate of change in overbank deposition associated with a distance equal to the channel half-width. The evolutions of levee taper associated with deposition by all 24 currents are presented in Figure 10, which clearly shows a cumulative increase in taper as the total thickness of the levee deposit grew. The final values for levee

experiment the slope was very close to zero. After passage of the 24 currents the average downstream centerline slope had increased to 0.013 m/m. Deposit sorting improved with distance traveled as $D90$ decreased by 40 μm over the study reach while $D10$ decreased by only 10 μm (Fig. 8). Superimposed on these basic streamwise trends are systematic, cross-channel variations in deposit thickness and its accompanying particle size. In every bend the location of the thickest and coarsest grain deposit was always displaced laterally from the centerline toward the outer bank (Figs. 6 and 8). To compare the magnitude of this skewing we digitized the path of maximum deposit thickness and grain size in the experimental channel from cross sections oriented perpendicular to the channel centerline (Fig. 9). The path of maximum particle size defines the crossover from inner to outer bank as occurring just

downstream from the points of channel inflection. These points of crossover are associated with a narrowing or necking of the contour lines defining the coarsest grain deposit on the channel bottom (Fig. 8B).

Sediment deposition was not limited to the bed of the channel. Sediment also accumulated on the channel sidewalls. During early flows the sediment deposited on the steep sidewalls (45°) was unstable and remobilized as grain flows that accumulated at the base of sidewalls. Remobilization of some fraction of sidewall deposits continued until the sidewall had been completely regraded to a new slope of ~21°, close to the particle angle of repose. Sediment layers deposited by currents following the regrading were not remobilized as grain flows (Fig. 5). Regrading of the sidewall slopes systematically reduced the width of the channel bottom (Fig. 5).
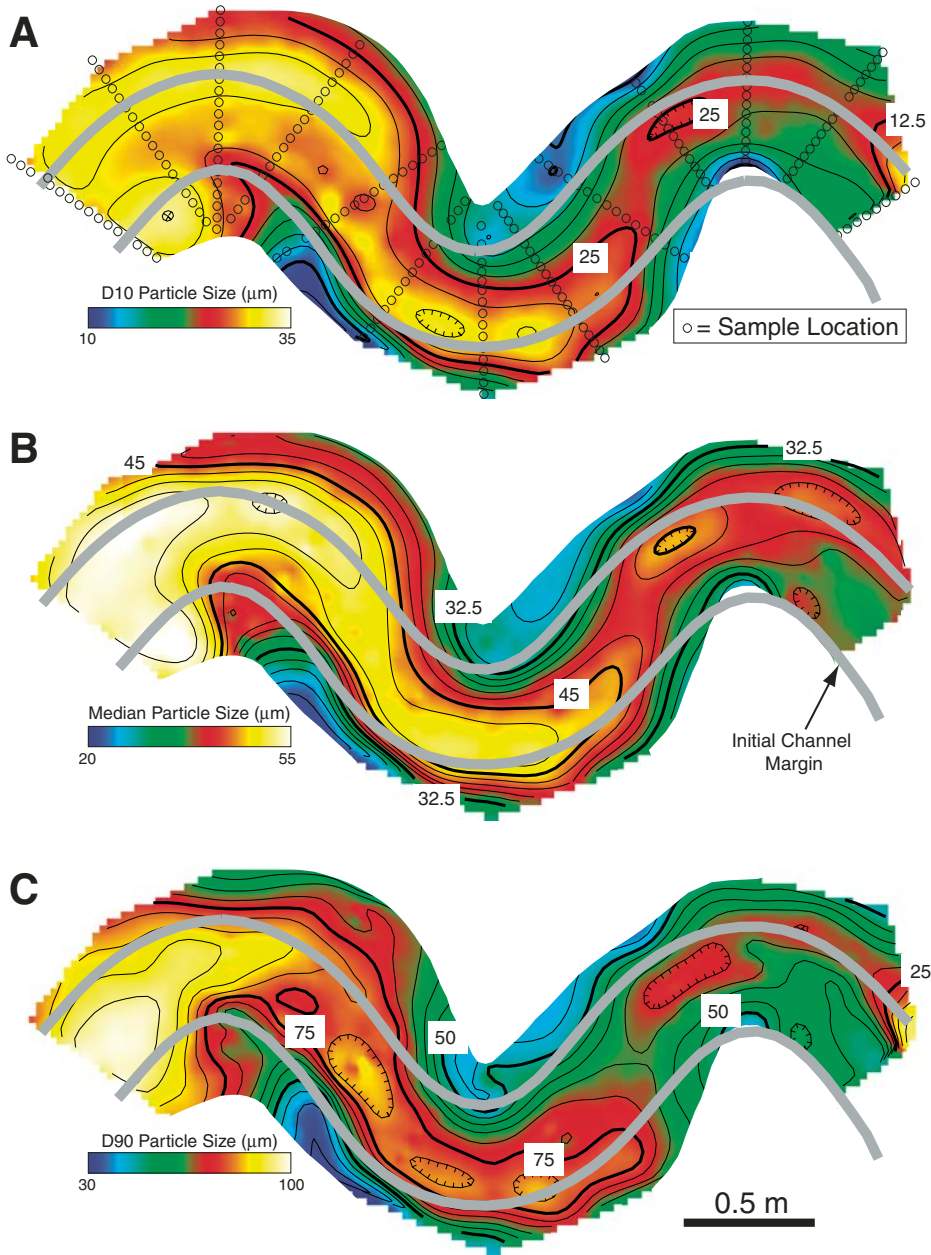
Figure 8. Maps of particle size for the total sedimentary deposit. Circles in A mark the 211 locations where vertically integrated sediment samples were collected for particle size analysis. Channel flow was from the left to the right in each map. (A) Nominal diameter, D, associated with particles composing the 10th percentile of the local deposit ($D10$). Contour interval is 2.5 μm. (B) Nominal diameter associated with the median particle size for the local deposit ($D50$). Contour interval is 2.5 μm. (C) Nominal diameter associated with particles composing the 90th percentile of the local deposit ($D90$). Contour interval is 5.0 μm. Gray bold lines in all three maps represent location of initial channel margin.
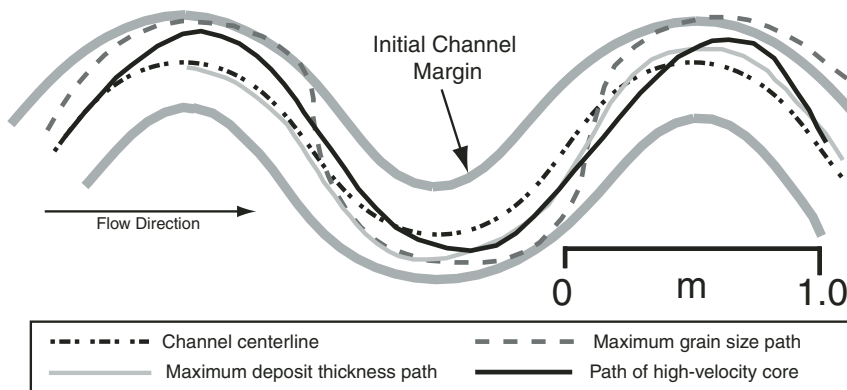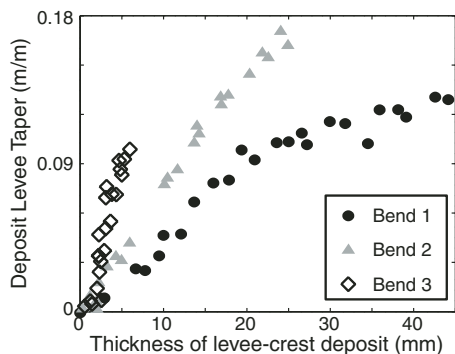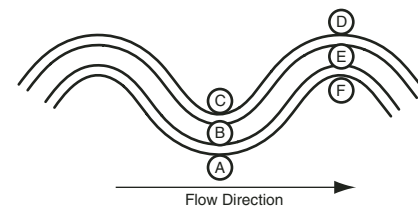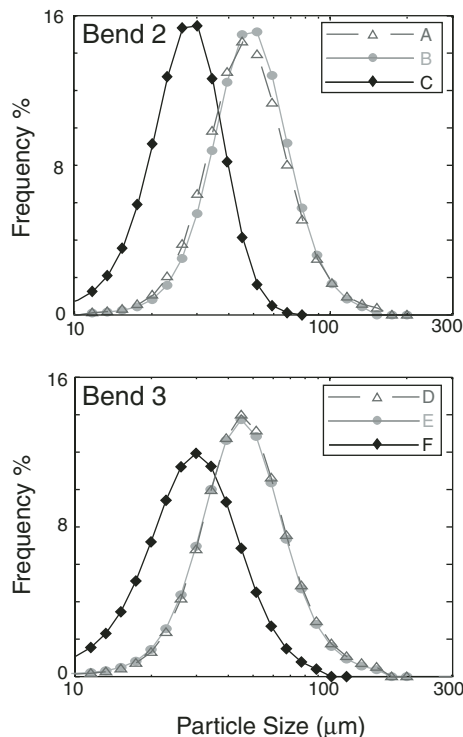

Figure 9. Downstream paths of maximum deposit thickness, maximum particle size, and high-velocity core compared to the channel centerline. Path of high-velocity core represents average path of high-velocity core measured for flows 2, 4, 8, 10, 11, 12, 13, 15, 17, 20, and 22.

Figure 10. Change in the levee-deposit taper as a function of deposit thickness at the levee crest. Measurements were collected following each current at the locations marked ADP1 (bend 1), ADP3 (bend 2), and ADP5 (bend 3) in Figure 4A.

Figure 11. Measured particle-size distributions for deposits at the apexes of bends 2 and 3. Location for each sediment sample is shown on the map at the bottom of the figure. At bend 2 there was essentially no difference in grain size between the outer-bank levee crest (A) and the channel bed at the centerline (B). Sediment deposited on the inner-bank levee crest (C) was substantially finer grained than A and B. At bend 3 there was essentially no difference in grain size between the outer-bank levee crest (D) and the channel bed at the centerline (E). Sediment deposited on the inner-bank levee crest (F) was substantially finer grained than at the outer-bank (D) and centerline (E).

taper at the outer banks of bends 1, 2, and 3 were 0.13, 0.17, and 0.11, respectively. These values are substantially different from values associated with inner-bank overbank deposits at the apexes of the three bends. Final values for levee taper at the inner banks of bends 1, 2, and 3 were 1.5×10^{-3}, -16.1×10^{-3}, and -2.9×10^{-3}, respectively. Overbank deposits at the inner banks of bends were characterized by approximately constant local thicknesses rather than wedge-like cross-sectional geometries (Fig. 5). These thicknesses represented only a fraction of the accumulation measured directly across the channel. The ratios of the inner to outer levee-crest deposit thickness taken at the apexes of bends 1, 2, and 3 were 3.2, 6.0, and 4.6, respectively.

Particle analyses of inner- and outer-bank levee deposits establish spatial patterns in grain-size distribution (Fig. 8) that are consistent with the previously described levee geometries. Particles composing the levee-crest deposits at the outer banks of bends are consistently coarser grained than the channel-edge deposits located directly across the channel on the inner bank (Fig. 11). The outer-bank deposits are so coarse as to be indistinguishable in composition to deposits laid down on the bed of the channel. All sizes of particles available for deposition on the channel bottom were also available for constructing the crests of outer-bank levees. The same condition did not hold for the distribution of particles composing the inner-bend overbank deposits. The coarsest particles found at the bed of the channel are not present at the inner banks of bends (Fig. 11). This difference between the particle-size distributions mirrors the difference in deposit thickness at inner- and outer-bank levee crests. Differences in the cross-sectional geometry of inner- and outer-bend overbank

deposits are also reflected in their particle compositions. Figure 12 summarizes these grain-size trends by focusing on the apexes of bends 1 and 2. The outer-bank deposits possess systematic reductions in median particle size with distance away from the channel edge. Inner-bank deposits display no trend with distance from the channel. These spatial trends in median particle size emulate the measured values for levee taper along the outer and inner banks of the channel.

Successive measurements from all three outer-bank levee deposits show that bend 1 evolved differently from bends 2 and 3. The total amount and grain size of sediment deposited at the outer bank of bend 1 increased with each flow while these properties remained approximately constant at the two downstream bends. These differences in levee evolution are highlighted by comparing bend 1 with bend 3 in Figure 13. Deposit thickness at the bend 1 levee crest remained a roughly constant 9 mm per flow for the first six currents and then began to systematically increase with each current thereafter (Fig. 13A). The final current deposited a 15-mm layer of sediment on the outer-bank levee of bend 1. In comparison, no temporal trend in deposition rate was observed at bend 2 and bend 3. For example, a roughly constant deposition rate of 6×10^{-1} mm per flow was measured for all 24 currents on the outer-bank levee of bend 3 (Fig. 13A). These temporal changes in levee deposition rate are matched by temporal changes in median particle size of the

levee deposits. The grain size of levee deposits increases from the early to intermediate and then later currents at bend 1 (Fig. 13B), whereas no such change was measured at bends 2 and 3. For example, levee deposits associated with the early, intermediate, and later currents record essentially no change in median particle size at the outer bank of bend 3 (Fig. 13B).

Changing Channel Morphology

The rate of sediment deposition on the bed of the channel always exceeded the rates of deposition on the adjacent overbank surface. As a result, the local channel depth or relief decreased at each point along the centerline throughout the experiment. We define this relief as the difference in elevation between the highest levee crest and the channel centerline. The bed of the channel at the entrance to the study reach had aggraded to an elevation nearly 75% of the original channel depth by the end of the experiment while maintaining ~50% of its original local relief. The channel bed at the end of the study reach aggraded only 34% its original depth, but retained 75% of its relief. Channel relief was preserved because losses due to sedimentation on the bed were offset by levee construction. Figure 7B shows three local maxima in channel relief that correspond to local maxima in levee deposition at the outer banks of bends 1, 2, and 3. Rapid levee growth along the outer banks of these bends slowed the loss of channel relief and
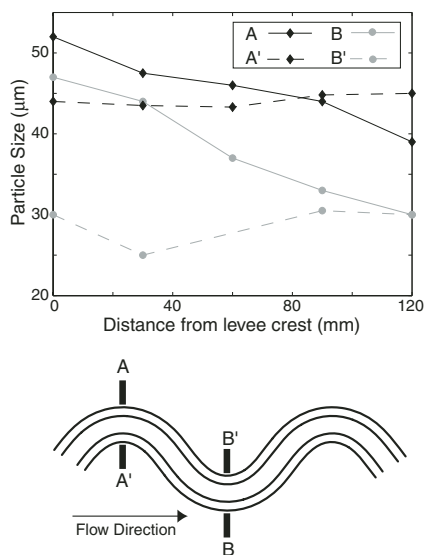
Figure 12. Change in median particle size of levee deposits as a function of distance from the levee crest. Solid lines indicate measurements taken from the outer banks of channel bends 1 and 2, and dashed lines indicate measurements from inner banks of the bends. Locations of these transects are drawn on the map at the bottom of the figure.

thereby maintained channel integrity at the very locations where currents are most likely to exit the channel. The local minima in channel relief correspond to the inflection points between the three bends.

Preferential sediment deposition along the outer banks of channel bends led to an asymmetry in channel cross-sectional shape (Fig. 5). This preferential deposition on one side of bends also produced a relative straightening of the channel centerline and a 3% reduction in channel sinuosity over the course of the experiment. The small change in plan form is associated with an average vertical displacement of the channel bed equal to nearly one-half of its original depth. This vertical climb with little distortion of the channel plan form is very similar to evolutions of many submarine sinuous channels (Hackbarth and Shew, 1994; Kneller, 2003; Peakall et al., 2000; Posamentier et al., 2000; Stelting et al., 1985).

Flow Velocity Data

Velocity profiles were collected at the inflection point between bends 1 and 2 for currents 2, 3, 4, 14, and 16 and at the inflection point between bends 2 and 3 for currents 17, 19, and 23 (Fig. 6A). The PCADP was located directly above the channel centerline at a constant

elevation that was ~0.5 m above the initial channel bed. Measurements were collected looking upstream in the direction of the channel centerline. Resulting profiles of mean streamwise velocity for these currents are presented in Figure 14. Estimates of current thickness using the velocity profiles collected at site ADP2 (Fig. 6A) show that this property was relatively insensitive to change in local channel relief. Total current thickness for flows 2, 3, and 4 was $1.12 \pm 0.08 \times 10^{-1}$ m and for flows 14 and 16 was $0.96 \pm 0.08 \times 10^{-1}$ m. Local channel relief associated with these same five currents is 0.109 m, 0.106 m, 0.103 m, 0.077 m, and 0.073 m. The maximum velocity associated with these five currents shows no systematic variation and was measured as $1.16 \pm 0.17 \times 10^{-1}$ m/s. Local channel relief at site ADP4 (Fig. 6A) was measured to be 0.078 m, 0.074 m, and 0.069 m for currents 17, 19, and 23, respectively. No systematic change in total current thickness or maximum velocity can be resolved between these series of flows, and they are simply measured to be $1.05 \pm 0.08 \times 10^{-1}$ m and $1.24 \pm 0.13 \times 10^{-1}$ m/s (Fig. 14B). In summary, there are essentially no resolvable changes in current thickness or maximum velocity between the sites ADP2 and ADP4 (Fig. 6A), even though the channel form evolved. The only notable change was in the structure of the velocity profile between the two measurement sites. Profiles collected at site ADP4 consistently had lower values for streamwise velocity above the velocity maximum than were measured at site ADP2 (Fig. 14).

The path of the high-velocity core was measured using overhead digital video of dye pulses injected into the body of flows 2, 4, 8, 10, 11, 12, 13, 15, 17, 20, and 22. For each flow the location of the leading edge of a dye pulse was digitized every second from the time of dye release until the dye pulse front reached the channel exit. The average path of the high-velocity core from the 11 measured flow paths is compared to the channel centerline, path of maximum deposit thickness, and grain size in Figure 9. The high-velocity core crosses the channel centerline a short distance upstream from the apexes of bends 1, 2, and 3. Maximum lateral separation between the position of the high-velocity core and the channel centerline occurs slightly downstream from the apexes of bends 1, 2, and 3 (Fig. 9).

Flow moving out onto the overbank surface at the outer banks of bends 1 and 3 was monitored with the PCADP during currents 5, 6, 7, 10, 12, 13, 15, 20, 22, and 24 (Fig. 6A). As has already been described, the sampling direction for the PCADP at locations ADP1, ADP3, and ADP5 (Fig. 6A) was aligned with the direction of the maximum horizontal overbank velocity at each point as mapped out from sequential overhead
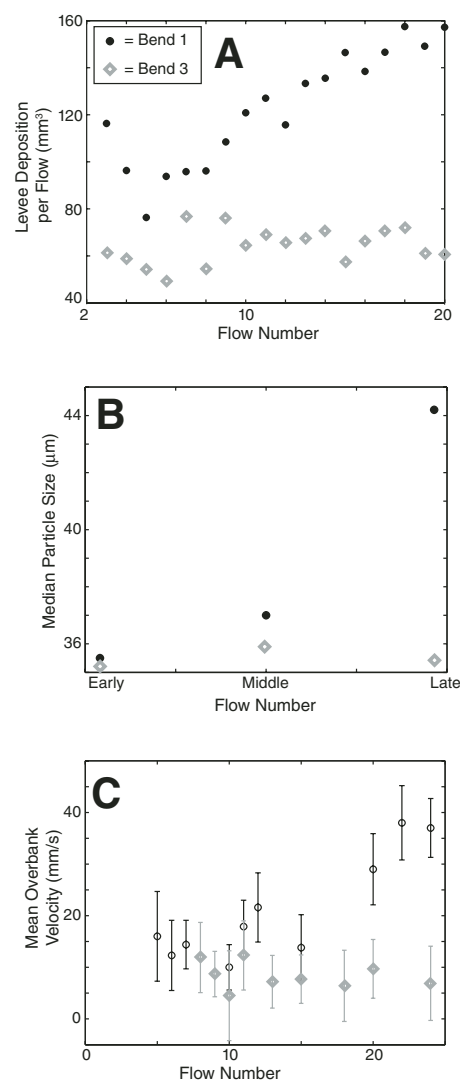
Figure 13. Temporal change in levee construction and levee-constructing flows at the outer banks of bends 1 and 3. These locations for bend 1 and bend 3 are labeled as sites ADP1 and ADP5 in Figure 4A. (A) Volume of sediment deposited on the proximal levee as a function of current number. The volume corresponds to a swath of levee measured from 0.3 m upstream to 0.3 m downstream of the bend apex. Each point here represents a boxcar averaging of deposit from three successive flows. (B) Median particle size for the levee crest deposit on the outer bank of bend apexes 1 and 3. (C) Vertically averaged velocity for flow moving out across overbank surface at sites ADP1 and ADP5 (Fig. 4A). Velocity was measured using the pulse-coherent acoustic-Doppler velocity profiler (PCADP), and reported error bars represent plus and minus one standard deviation in the values for mean velocity collected every 4 s throughout the duration of each flow.

A 1st Inflection Point
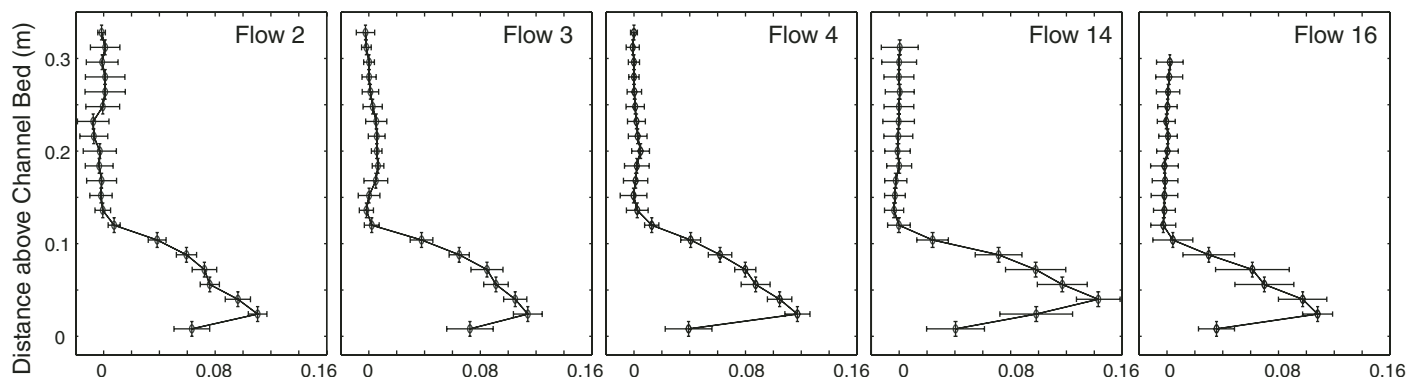
B 2nd Inflection Point

Streamwise Velocity (m/s)
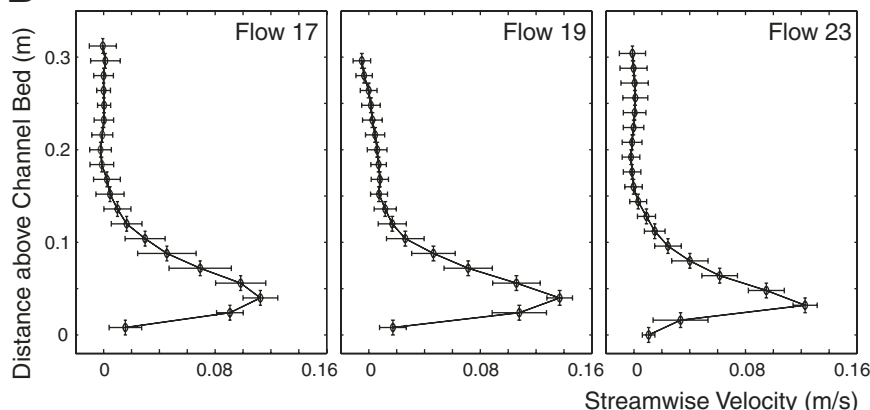
Figure 14. Profiles of downstream velocity for various currents measured at the channel centerline using the pulse-coherent acoustic-Doppler velocity profiler (PCADP). Vertical error bars define the extent of each sampling volume while the horizontal error bars are plus and minus one standard deviation calculated using all values for current velocity collected in each sampling volume. (A) Velocity A. (B) Velocity profiles for currents measured at the channel inflection point marked ADP4 in Figure 4A.

video images of the leading edge of injected dye pulses. At the apex of bend 1 (ADP1), the mean current velocity for overbanking flow steadily increased from ~0.015 ± 0.009 m/s early in the experiment to 0.035 ± 0.006 m/s near the end of the experiment (Fig. 13C). This increase is associated with a decrease in channel relief at bend 1 from 0.098 m to 0.060 m. No equivalent change in mean overbank velocity was measured at bend 3 (ADP5, Fig. 13C). The local overbank velocity here maintained a nearly constant value of 0.009 ± 0.007 m/s, even though the local channel relief dropped from 0.099 m to 0.075 m between currents 5 and 24.

Zones of Flow Separation

Zones of low flow velocity along portions of the inner banks of bends were resolved using injections of dye into the bodies of currents. Video of these injections documents current separation from the inner wall at the bend apex and its reattachment to the sidewall just downstream from the inflection point. This separation produces a lag in the arrival of dye to the interior of these zones followed by a lag in its release back to the core flow, at which time it is rapidly

advected out of the system (Fig. DR1; see footnote 1). The positioning of these separation zones coincides with the lateral displacement of the high-velocity core toward the outer bank of each bed (Fig. 9). Flow in these separation zones possesses an interesting but largely unresolved complication associated with some minor amount of overbank flow reentering the channel at these locations. This movement of overbank flow back into the channel is visualized in Figure 3 and Figure DR1 (see footnote 1). The effect of the low-velocity zones on channel depositional patterns is discussed in a later section.

Current Superelevation

The upper surface of a turbidity current at any channel cross section was not associated with a single elevation but varied laterally between channel banks as a function of channel curvature. In this study we focused on the surface elevation at channel-bend apexes and specifically measured the change in surface elevation for the current at the outer channel bank and the channel center line. Following Engelund (1974) and Imran et al. (1999), we call this cross-stream variation in surface elevation the current

superelevation. Measuring the local surface elevation is a two-step process. First, local current thickness was measured using the PCADP. This thickness is then transformed into an elevation by adding it to the local bed topography. Local surface elevations were measured at locations marked ADP2, ADP3, ADP4, and ADP5 in Figure 6. This calculation uses the surface elevation measured at the inflection point as a proxy for the centerline elevation at the bend apex. This assumption is supported by the nearly constant current thickness measured at the 1st and 2nd inflection points. Using these measurements, current superelevations of 34 ± 8 mm and 26 ± 8 mm are estimated for the 2nd and 3rd bends, respectively, which equates to ~25% of the total current thickness at the channel centerline.

An independent estimate of current superelevation was made using overhead photography. Injected dye images were converted into maps of current thickness using the Lambert-Beer law of light absorption:

$$I = I_0 10^{-\alpha l c} \qquad (4)$$

where *I* is intensity of dye after passing through a given material, I_0 is the maximum intensity

of dye, α is an absorption coefficient, l is the distance light passes through material, and c is the concentration of absorbing species (Starn, 1981). For our analysis, we injected red dye into currents and measured the intensity of red in images collected from stills of digital video defined by red, green, and blue color maps. For each analyzed image, we subtracted the intensity of red dye present in a video frame prior to the injection of the dye. We assume an I_0 of 255 on a red, green, and blue color map. Values for α and c are then calibrated at locations where current thickness has been measured with a PCADP. Rearranging equation 4 to solve for l allows us to create maps of current thickness from frames of digital video. Maps of current thickness were then added to local topography to create maps of surface elevation associated with the top of the current. This method gives a superelevation of 49 mm at the 1st bend and 47 mm at the 2nd bend. Plots showing the superelevation at the apexes of bend 1 and 2 are presented in Figure 15.

INTERPETATION

Superelevation in Channel Bends

The superelevation of flows measured at bends 2 and 3 was approximately equal to 25% of the total current thickness. This fraction is large compared to those measured for flows in river bends. For example, field measurements by Dietrich and Whiting (1989) resolve a superelevation equal to 1% of the total flow depth, and laboratory data analyzed by Smith and McLean (1984) show a superelevation equal to only 8% of the mean flow depth. In order to understand these differences in degree of cross-channel superelevation it is prudent to revisit the dynamics of channelized flow that produce it, beginning with rivers. The cross-stream difference in water surface elevation at river bends is a well-known phenomenon typically ascribed to the balance between a centrifugal force and a restoring pressure gradient force (Engelund, 1974; Johannesson and Parker, 1989; Rozovskii, 1961; Yen and Yen, 1971). Describing superelevation solely as the consequence of this balance is a result of the manner in which the equations of motion for flow in a bed have traditionally been simplified to make them amenable to stability analyses (Nelson and Smith, 1989). Specifically, it has been assumed that vertical velocities are negligible and the equation describing the balance of vertical momentum in the flow can be reduced to the hydrostatic condition, a condition requiring that vertical accelerations be sufficiently small that they can be set to zero without accumulating significant error (Nelson and Smith, 1989). It is recognized that this simplification to the flow

field accrues significant error in the vicinity of steep channel sidewalls, where vertical accelerations are always important, but these nonhydrostatic effects have been left out of full descriptions for the flow field by arguing that these defects are local in nature, have a small effect on the overall flow pattern, and their addition would complicate the theory substantially from a mathematical point of view without adding much new physical insight (Johannesson and Parker, 1989; Smith and McLean, 1984). The developing theory of Imran et al. (1999) and Corney et al. (2006) has adopted this simplifying assumption of a hydrostatic condition to the flow of turbidity currents in channel bends. Our laboratory data call into question the use of this simplifying assumption by highlighting patterns of flow and sedimentation that are consistent with significant vertical accelerations associated with runup of the high-velocity cores of currents onto channel sidewalls. In the subsequent sections, we explore the various forces contributing to the large superelevations seen in our experiment.

Centrifugal Contribution

The cross-stream difference in water surface elevation observed in river bends is typically ascribed to the balance between a centrifugal force and a restoring pressure gradient force (Engelund, 1974; Johannesson and Parker, 1989; Rozovskii, 1961; Yen and Yen, 1971). This relationship is based on two assumptions: (1) all fluid remains contained within the channel while traversing the bend and (2) streamlines always run parallel to the channel centerline and banks (Engelund, 1974; Johannesson and Parker, 1989; Rozovskii, 1961; Yen and Yen, 1971). In this framework, cross-channel flow can only be produced by a centrifugal force. The surface slope balancing this outward directed flow is:

$$S = \alpha \frac{H}{r_0 Fr^2}, \qquad (5)$$

where r_0 denotes the channel centerline radius of curvature and α is a parameter very near unity (Engelund, 1974; Johannesson and Parker, 1989; Rozovskii, 1961). This equation can be rearranged to solve for current superelevation, Δz, measured between the channel centerline and outer bank:

$$\Delta z = \alpha b \frac{\bar{u}^2}{2r_0 \left(\frac{\rho_c - \rho_a}{\rho_c} \right) g}. \qquad (6)$$

Using equation 6, a superelevation of 14 mm is predicted at the apexes of our experimental bends. Parameters used for this calculation are $r_0 = 0.59$ m, $b = 0.40$ m, $\bar{u} = 0.08$ m/s, $\rho_c =$
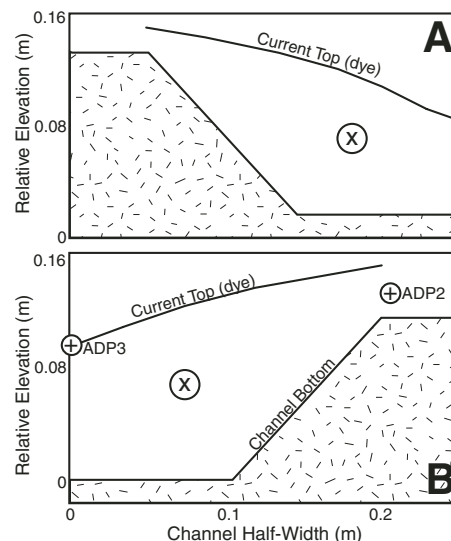
Figure 15. Measurements defining current superelevation at bends 1 and 2. (A) Estimate of cross-channel elevation for the top of a current from analysis of dye injections recorded by overhead photographs at bend 1. This analysis suggests that the top of the current at the outer channel bank (x = 0.2 m) is elevated 4.9 cm above the top of the current at the channel centerline (x = 0 m). (B) Estimate of cross-channel elevation for the top of a current from both dye-injection analysis and direct detection at bend 2. Dye analysis suggests that the top of the current at the outer channel bank (x = 0.2 m) is elevated 0.047 m above the top of the current at the channel centerline (x = 0 m). Relative elevations for the current top measured using the pulse-coherent acoustic-Doppler velocity profiler (PCADP) are labeled points ADP2 and ADP3. These point measurements define a difference in elevation between the outer bank and channel centerline of 0.024 cm.

1016 kg/m³, and $\rho_a = 1000$ kg/m³. Values for ρ_c and $\bar{u}$ are for measured conditions at the inflection point between bends 2 and 3.

Estimates of current superelevation using equation 6 substantially underestimate the measured values. The estimated value is only 41% of the current superelevation at bend 2 and 54% at bend 3. This underestimate is not surprising given the fact that streamlines were observed to cross the channel centerline (Fig. 9) and a portion of the current exited the channel along the outer bank of each bend (Fig. 3), therefore violating the assumptions in equations 5 and 6. The circulation direction of helical flow in submarine channel bends has been debated in

recent laboratory (Corney et al., 2006; Imran et al., 2007) and computational studies (Kassem and Imran, 2005). These studies focus on the sense of cross-stream flow resulting from flow superelevation and associated implications for sediment transport. We investigate movement of the basal current up the outer sidewall and out of the channel resulting from runup of turbidity currents in the following section. The consequences of runup on patterns and compositions of overbank deposits are also presented.

Runup Contribution

The experiment provides clear evidence for superelevation resulting from the runup of currents onto the outer banks of all channel bends. Particle size data from deposits record this runup of the basal part of the currents onto outer sidewalls in all bends, as seen in Figure 8. In addition, this runup is captured by the path of the high-velocity core relative to the channel centerline (Fig. 9). At channel bends the high-velocity core deviates from the channel centerline, and moves toward the outer channel bend wall. This runup can be understood by simply balancing the kinetic energy of a current against the potential energy gained as it moves up a sloping sidewall (Chow, 1959; Hungr et al., 1984; Kirkgoz, 1983). Any parcel of current has a kinetic energy per unit volume equal to $\frac{1}{2}\rho_c u_2$, and an associated maximum runup height, Δz, associated with its kinetic energy being completely converted to a potential energy equal to $(\rho_c - \rho_a)g\Delta z$. The resulting expression for Δz is

$$\Delta z = \frac{\rho_c u^2}{(\rho_c - \rho_a)2g}, \qquad (7)$$

and represents an upper limit to the runup elevation because energy losses due to friction are neglected. We estimate maximum runup by calculating Δz specifically associated with the high-momentum cores of currents. To do this, we use measured values of $u = 0.11$ m/s, $\rho_c = 1019$ kg/m³, and $\rho_a = 1000$ kg/m³. Inserting these values into equation 7 yields $\Delta z = 33$ mm at bend apexes. The measured superelevation of currents in bends exceeds that calculated with either equation 6 or 7. Clearly additional study is required to fully understand the cross-channel flow within turbidity currents moving through channel bends.

Implications for Flow Splitting

Observations of current runups at outer banks of bends are inconsistent with the proposed occurrence of flow splitting that assumes that the discharge lost at bends is restricted to some upper fraction of the currents (Peakall et al., 2000; Piper and Normark, 1983). This interpretation is untested and not consistent with grain size data collected on the bed of the channel and the levee crest (Figs. 8 and 11). These data seem to require that the basal current become elevated to the height of the levee crests at all three bends. The resultant overbank flow had a composition equivalent to that of the entire channelized current rather than only some upper portion. We acknowledge that flow splitting can occur, but data from this experiment show that the flow-splitting model does not always provide an accurate description for the compositional evolution of currents traversing sinuous channels. Replacement or placement of limits on the applicability of the flow splitting model to these systems has important implications for which particle sizes are tapped by overbank sedimentation, and therefore the composition of a channelized current with distance from its source.

Recent studies investigating turbidity current flow in channel bends have focused on cross-channel flow driven by the balance between a centrifugal force and a restoring pressure gradient force (Imran et al., 2007; Keevil et al., 2006). These studies highlight how complicated the structure of the cross-channel circulation pattern can be given typical profiles for density and streamwise velocity in turbidity currents and the possible entrainment of overlying ambient fluid into currents. Our study shows nearbed cross-channel flow affecting sedimentation patterns in bends is not always primarily related to the restorative balance between centrifugal force and pressure gradient force. Runup provides another mechanism for transport of coarse sediment to the outer banks of channel bends. Our observations of the path of the high-velocity core, deposit particle-size patterns, and estimates of superelevation using equation 7 suggest that in some cases runup can be the dominant cross-channel transport mechanism in bends. The presence of current runup and significant vertical velocities at channel bends also highlights the importance of channel sidewall angles to the interaction of turbidity currents with channel forms.

First Bend as a Filter

Systematic increases in mean overbank velocity and levee crest sedimentation were measured for successive currents at the first bend (Fig. 13). These same properties did not vary throughout the experiment at bends 2 and 3. This difference suggests that the first bend acted as a filter on currents traversing the sinuous channel. The thickness of each current as it entered the channel was

~0.12 m. At the beginning of the experiment, this thickness approximately matched the local channel relief, but sediment deposition by successive currents partially infilled the channel and decreased this relief. This resulted in a greater fraction of the current being elevated above the levee crest as it entered the first bend, where it spilled onto the overbank surface, resulting in the trends seen in Figure 13. The increasing amount of overbank sedimentation, the coarsening of the overbank deposit, and the increasing velocities for the overbank flow are all consistent with an ever greater fraction of a current exiting the channel at this position. This loss of current at the first bend reduced the discharge of the remaining channelized flow, producing a current that was roughly compatible with the cross-sectional area of the evolving channel. The lack of systematic trends in overbank sedimentation and the flow measured at bend 2 and bend 3 (Fig. 13) are consequences of these adjusted currents. The substantial differences between the measured trends at bend 1 versus bend 2 and bend 3 illustrate the effectiveness of a single bend as a filter on passing currents.

This experimental result highlights an internal process that almost certainly limits the variability in properties of turbidity currents traversing sinuous submarine channels. In particular, this filter is envisioned to reduce the natural variability in current discharges entering a system by adjusting higher discharge cases. Laterally confined currents in canyons that empty into aggrading sinuous channel forms can be expected to undergo adjustments to their discharge over a small number of high-amplitude bends. This process of current filtering by channel bends might provide a partial explanation for the slowly varying dimensions of many aggrading leveed submarine channels with distance down slope (Pirmez and Imran, 2003).

DISCUSSION

Control of Curvature on Channel Evolution

One of the most striking results of this experiment is the high deposition rates that occur along the outer banks of bends. This sedimentation pattern is quite different than expected patterns of deposition in sinuous rivers (Engelund, 1974; Imran et al., 1999; Rozovskii, 1961; Yen and Yen, 1971) (Fig. 16), but compatible with results from a numerical model for fully channelized turbidity currents by Das et al. (2004). We think the differences in patterns are the result of differences in the primary mode of sediment transport in the two environments. In rivers bedload transport dominates the evolution of channel morphology, including the
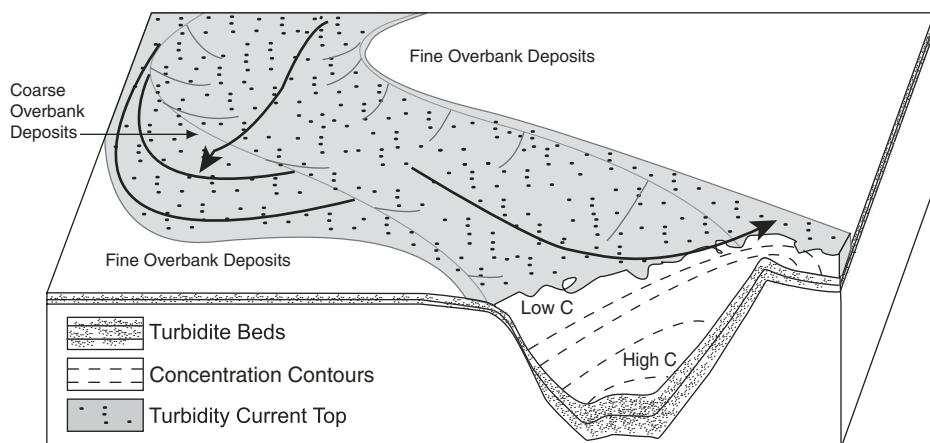
Figure 16. Schematic illustration of turbidity current flow in a sinuous channel. Arrows indicate direction of overbanking flow. Greater deposition occurs on outer bank relative to inner channel bank as a result of runup.

development and growth of point bars (Deitrich and Whiting, 1989). Bedload transport does not cover the relatively steep outer banks of bends, leaving these sidewalls exposed to erosion by the moving fluid. A depositional turbidity current can mantle the entire channel form with a layer of sediment that settled onto the bed from suspension. These layers dominate the stratigraphy of our experimental channel, confirming that fallout of grains carried in suspension primarily controlled the morphological evolution of our channel. Following Das et al. (2004), we conclude that sedimentation rates were greatest where near-bed suspended-sediment concentrations were greatest, along the outer versus inner banks of channel bends. Higher deposition rates toward the outer banks of bends decreased channel sinuosity from 1.32 to 1.27 over the course of the experiment. This reduction in sinuosity was associated with the nearly vertical climb of the channel form. Channels that aggrade vertically with little change in their planform are commonly observed on the seafloor (Hackbarth and Shew, 1994; Peakall et al., 2000; Posamentier et al., 2000). The close connection between aggrading channel forms and minimal change in channel sinuosity strongly suggests that the production of sinuosity must be associated with net-erosional or nondepositional turbidity currents (Das et al., 2004).

Zones of flow separation were observed at the inner banks of bends immediately downstream from bend apexes, even though the experimental channel was smoothly varying in form and had a constant width. Sediments that accumulated in these low-velocity zones situated between the points of flow separation and reattachment had different properties than those deposited on the floor of the adjacent active channel. Measurable

differences were observed in the deposit thickness and in the sizes of the accumulating grains. The beds of separation zones were consistently finer grained than deposits accumulating in the active channel (Fig. 8). This difference is similar to what is observed in rivers where the grain-size reduction in the low-velocity zones is a consequence of how sediment-laden flow is transferred into the separation zones (Makaske and Weerts, 2005; Nanson and Page, 1983; Schmidt et al., 1993). These separation-zone deposits are enriched in particle sizes that are fully suspended throughout the water column and are advected into the low-velocity zones, where they settle out and aggrade the bed. Sedimentation within these lower-velocity separation zones often leads to the construction of positive topography that in alluvial rivers is commonly referred to as a concave bench (Makaske and Weerts, 2005; Nanson and Page, 1983; Schmidt et al., 1993). Positive topography similar to a concave bench was not observed for the zones associated with bends 2 and 3 of our experimental channel (Figs. 5B, 5C, and 6C). Instead these zones developed into topographic lows because sedimentation there was ~70% of that in the adjacent channel. Sedimentation was greater in the active channel than in these two separation zones, even though current velocities were greater in the active channel compared to the separation zones. In order to understand this result it is important to remember that every turbidity current was depositional, mantling the entire bed with a layer of sediment. For this case, local sediment deposition was predominantly controlled by the volume concentration of particles suspended above that bed location and their settling velocities (e.g., Das et al., 2004). Figure 9 shows that both the high-velocity and sediment-charged

cores of the turbidity currents were shifted laterally away from the separation zones in bends 2 and 3, toward the outer bank. There was simply less sediment available with these low-velocity zones to rain out from suspension and raise the bed level. Figure 8 clearly shows that a wider range of particle sizes was available to aggrade the bed of the active channel compared to the beds of the separation zones. This wider range of available grain sizes translated into somewhat greater deposition rates. Determining the mechanisms limiting transport of suspended sediment from the core flow into inner-bank separation zones is a topic of future research. In our experiment, sediment deposition by turbidity currents in the active channel exceeded that associated with sediment trapped in the separation zones. We speculate that sediment transferred into separation zones will construct positive, bar-like topography in those cases where the turbidity currents deposit much less or no sediment on the bed of the active channel. We propose that zones of flow separation are common in natural submarine channels, and accurate interpretation of deposits accumulated on the inner banks of bends requires considering the possibility that this sedimentation occurred in such zones of low current velocity.

Submarine Levee Construction

Three-dimensional seismic imaging of submarine channels has provided the geological community with a great deal of geometric data defining the structure of levees and associated overbank deposits (Clemenceau et al., 2000; Pirmez and Flood, 1995; Skene et al., 2002). Measured levee tapers from several natural systems compare favorably to tapers of levees deposited during our experiment (Fig. 17). Unfortunately the wealth of geometric data is not matched by a comparable quantity of core, outcrop, or experimental data characterizing the composition of these deposits or the processes through which they are constructed, with notable exceptions, including Mohrig and Buttles (2007) and Mohrig et al. (2005). Inverting for overbank processes using particle size measurements from cores is difficult because most cores that sample levees have been collected several kilometers from the channel axis (Hiscott et al., 1997; Pirmez et al., 1997). One exception is found in core and seismic data presented by Clemenceau et al. (2000) showing that levee deposits from the Ram-Powell field in the Gulf of Mexico are composed of particles with a size distribution that is similar to the associated channel-filling sands. Even with these data, Clemenceau et al. (2000) were unable to correlate individual overbank deposits to specific channel-filling deposits, as we report

[a]Skene, 1998; [b]Pirmez and Flood, 1995;
[c]Deptuck et al., 2003; [d]Demyttenaere et al., 2000
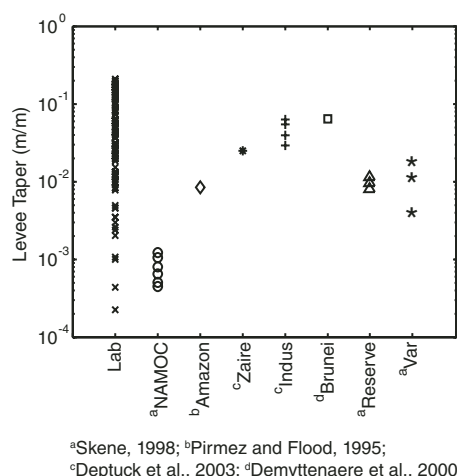
Figure 17. Comparison of experimental levee tapers following flow 24 with levee tapers measured from studies of 7 natural systems. NAMOC—North Atlantic Mid-Ocean Channel.

in the experiments herein. Outcrop studies that characterize the interaction of turbidity currents with channel bends are also rare due to the inherent difficulty in determining the position and orientation of a roughly two-dimensional exposure within a three-dimensional channel form (Gardner et al., 2003; Morris and Busby-Spera, 1990). However, an outcrop study of the Carboniferous Ross Formation in southwest Ireland concluded that the crests of levees built from the spillover of channelized currents were as coarse as the channelized deposits (Lien et al., 2003).

The present experimental results show a clear relationship between the character of the overbank flow and the geometry and composition of the levees that are constructed. The levees that develop on the inner banks of all bends are relatively thin, have small tapers (Fig. 5), and show little change in grain size (Fig. 12) with distance from the levee crest. All of these properties are consistent with well-mixed vertical profiles having little change in suspended sediment concentration and particle size with distance above the overbank surface. These current properties are representative of the relatively fine grained and dilute upper flow that resides above the channel where it was free to spread laterally, moving onto the overbank surface. A different structure was observed for the overbank flow at the outer banks of bends. Levees that developed at these sites were relatively thick, had high tapers (Fig. 5), and showed systematic reductions in grain size with distance away from the levee crest line (Fig. 12). All of these trends are consistent with construction by overbank flows having vertically stratified profiles for grain size and suspended-sediment concentration. As

previously stated, these profiles contain all of the particle sizes found in the basal channelized current, a consequence of current running up and out of the channel at the outer banks of bends.

The growth of levees at the outer banks of bends varied as a function of bend number. These changes can be related to the evolving suspended sediment profiles. Figure 10 shows that the amount of sediment available to build levees decreased from bend 1 to bend 3. This reduction in sedimentation was accompanied by a decrease in deposit grain size (Fig. 8). In spite of this, levee tapers remain high; this suggests that the stratification was preserved within the overbanking flow even when the amount and sizes of sediment are diminishing.

The construction of thick levees on the outer banks of bends plays an important role in preserving the channel relief through time. As shown in Figure 7B, construction of the outer bank levees keeps the local channel relief high at points where runup and loss of current are significant. This pattern of levee growth allowed the channel to remain a flow conduit while undergoing large amounts of vertical aggradation, a pattern often seen in acoustic images of submarine channels (Hackbarth and Shew, 1994; Posamentier, 2003).

Our experiment clearly shows a connection between the flow field, channel planform, and evolution of channel morphology. This result is in contrast to statements by Skene et al. (2002), whose study of natural levees on submarine channels concluded that there is no connection between local channel planform and levee morphology. The disagreement points out a need for the collection and analysis of additional data from natural and experimental channels as well as a need to collect data with sufficient resolution and density to confirm the presence or absence of these correlations.

Implications for Using Levee Heights to Estimate Current Velocities

Komar (1969) proposed a model that relates channel morphology to the physical characteristics of channel-building currents by using the differences in levee crest elevation at the outer and inner banks of bends as a proxy for current superelevation and connecting it to a centrifugal acceleration experienced by the channel-building currents with equation 6. This method was used by Pirmez and Imran (2003) to estimate characteristic current velocities in the sinuous Amazon Submarine Channel. The results of our study suggest that the simple force balance described by equation 6 underestimates the current superelevation and consequently, when used as an inversion tool, overestimates

current velocities. The estimates for mean current velocity in 12 channel bends described by Komar (1969) are 30% greater when using equation 6 versus equation 7. We understand that the runup expression for superelevation (equation 7) is incomplete, but it provides some measure of the possible systematic error associated with the Komar method. The result points to a need for continued investigation of flow in submarine channel bends with a variety of configurations. Only after this is completed can the depositional records preserved in levees be used to more accurately constrain seascape-forming conditions.

SUMMARY

In this experiment, we monitored the interactions between 24 turbidity currents and an aggrading sinuous channel. All currents were depositional, with sedimentation occurring by suspension fallout. This sedimentation systematically reduced channel relief because deposition on the channel bottom was always somewhat greater than that on the channel-bounding levees. The sedimentation pattern was skewed toward the outer banks of bends, which produced a slight reduction in sinuosity of the channel form as it aggraded. Sedimentation on the crest of levees at the outer banks of bends was 3–4 times greater than that found on the inner banks and enhanced deposition on outer banks minimized the reduction of channel relief at the sites where we measured the greatest loss of channelized current to the overbank surface. The growth of levees at the outer banks of bends helped preserve the integrity of the channel form to act as a conduit for future flows. A cross-channel asymmetry in deposit particle sizes was also measured. This asymmetry was large enough that levee crest deposits on the outer banks of bends were as coarse as sediment deposited in the channel thalweg.

The measured superelevations of currents across bend apexes are 85%–42% greater than values predicted using a standard balance between the centrifugal and pressure gradient forces (equation 6). Particle sizes on the channel banks point to a large runup of the currents at these zones of high curvature. We propose that the high superelevations measured in the experimental bends are a combination of the well-known centrifugal contribution and a runup associated with the momentum of a current (equation 7). Streamwise velocities for turbidity currents and rivers are comparable, but the runup of turbidity currents is significantly greater due to their low excess density when compared to the ambient fluid. The value of $\rho_c/(\rho_c - \rho_a)$ for rivers roughly equals 1, while this ratio for

turbidity currents ranges between 0 and 100. Its representative value for our experiment was 33. The large runup for turbidity currents and the deposition of coarse particles to the outer banks of our channel bends suggest that some portion of the basal current can exit the channel at bends. This result contradicts conceptual models of the downstream coarsening of currents due to flow splitting (Peakall et al., 2000; Posamentier and Kolla, 2003). Further studies are needed to quantify how changes in channel sinuosity affect the relative contributions of runup and the centrifugal force in setting the cross-stream superelevation. As long as direct measurements from turbidity currents remain few and technically difficult to obtain, results from this study and other channelized experiments will prove valuable in determining the interactions between currents and natural topography that lead to construction of the seascape.

ACKNOWLEGMENTS

APPENDIX

α	absorption coefficient
b	channel width
B_{f0}	buoyancy flux
c	concentration of absorbing species
C_f	bed friction coefficient
D	particle diameter
g	acceleration due to gravity
H	thickness of flow
Fr	Froude number
φ	angle of channel centerline relative to mean downstream direction
I	dye intensity
k	von Kármán's constant
L	distance light passes through material
Re	Reynolds number
Re_s	particle Reynolds number
r_0	channel centerline radius of curvature
R	submerged specific density
ρ_a	the density of the ambient water
ρ_c	the bulk density of the flow
S	slope
s	sinuosity
T	flow duration
τ_b	bottom shear stress
τ^*	dimensionless bed shear stress
u	streamwise velocity
u^*	shear velocity
υ	kinematic viscosity
w_s	particle settling velocity
ω	maximum angle channel centerline makes with mean downstream direction
x	downstream distance
X_t	total downstream meander length
z	height above channel bed
z_0	roughness parameter

REFERENCES CITED

Altinakar, M.S., Graf, W.H., and Hopfinger, E.J., 1996, Flow structure in turbidity currents: Journal of Hydraulic Research, v. 34, p. 713–718.

Bagnold, R.A., 1966, An approach to the sediment transport problem from general physics: U.S. Geological Survey Professional Paper 422-I, 31 p.

Bouma, A., 2000, Fine-grained, mud-rich turbidite systems: Model and comparison with coarse-grained, sand-rich systems, *in* Stone, G.G., ed., Fine-grained turbidite systems: SEPM (Society for Sedimentary Geology) Special Publication 68, p. 9–20.

Chow, V.T., 1959, Open-channel hydraulics: New York, McGraw-Hill, 680 p.

Clark, J., and Pickering, K., 1996, Architectural elements and growth patterns of submarine channels: Applications to hydrocarbon exploration: American Association of Petroleum Geologists Bulletin, v. 80, p. 194–221.

Clark, J., Kenyon, N., and Pickering, K., 1992, Quantitative analysis of the geometry of submarine channels: Implications for the classification of submarine fans: Geology, v. 20, p. 633–636, doi: 10.1130/0091-7613(1992)020<0633:QAOTGO>2.3.CO;2.

Clemenceau, G.R., Colbert, J., and Eddens, A., 2000, Production results from levee-overbank turbidite sands at Ram/Powell field, Deepwater Gulf of Mexico, *in* Weimer, P., et al., eds., Deep-water reservoirs of the world: GCSEPM Foundation 20th Annual Bob F. Perkins Research Conference, p. 241–251.

Corney, R.K.T., Peakall, J., Parsons, D.R., Elliott, L., Amos, K.J., Best, J.L., Keevil, G.M., and Ingram, D.B., 2006, The orientation of helical flow in curved channels: Sedimentology, v. 53, p. 249–257, doi: 10.1111/j.1365-3091.2006.00771.x.

Das, H., Imran, J., Pirmez, C., and Mohrig, D., 2004, Numerical modeling of flow and bed evolution in meandering submarine channels: Journal of Geophysical Research, v. 109, p. 1–17.

Demyttenaere, R., Tromp, J.P., Ibrahim, A., Allman-Ward, P., and Meckel, T., 2000, Brunei deep water exploration: From sea floor images and shallow seismic analogues to depositional models in a slope-turbidite setting, *in* Weimer, P., et al., eds., Deep-water reservoirs of the world: GCSEPM Foundation 20th Annual Bob F. Perkins Research Conference, p. 304–317.

Deptuck, M.E., Steffens, G.S., Barton, M., and Pirmez, C., 2003, Architecture and evolution of upper fan channelbelts on the Niger Delta slope and in the Arabian Sea: Marine and Petroleum Geology, v. 20, p. 649–676, doi: 10.1016/j.marpetgeo.2003.01.004.

Dietrich, W.E., and Whiting, P.J., 1989, Boundary shear stress and sediment transport in river meanders of sand and gravel, *in* Ikeda, K., and Parker, G., eds., River meandering: American Geophysical Union Water Resources Monograph 12, p. 1–50.

Engelund, F., 1974, Flow and bed topography in channel bends: Journal of Hydraulic Engineering, v. 100, p. 1631–1648.

Garcia, M.H., 1994, Depositional turbidity currents laden with poorly sorted sediment: Journal of Hydraulic Engineering, v. 120, p. 1240–1263, doi: 10.1061/(ASCE)0733-9429(1994)120:11(1240).

Gardner, M.H., Borer, J.M., Melick, J.J., Mavilla, N., Dechesne, M., and Wagerle, R.N., 2003, Stratigraphic process-response model for submarine channels and related features from studies of Permian Brushy Canyon outcrops, West Texas: Marine and Petroleum Geology, v. 20, p. 757–787, doi: 10.1016/j.marpetgeo.2003.07.004.

Graf, W.H., 1971, Hydraulics of sediment transport: New York, McGraw-Hill, 513 p.

Hackbarth, C.J., and Shew, R.D., 1994, Morphology and stratigraphy of a mid-Pleistocene turbidite leveed channel from seismic, core, and log data, northeastern Gulf of Mexico, *in* Submarine fans and turbidite systems, sequence stratigraphy, reservoir architecture and production characteristics: GCSEPM Foundation 15th Annual Research Conference, p. 127–140.

Hay, A.E., 1987, Turbidity currents and submarine channel formation in Rupert Inlet, British Columbia; 2, The role of continuous and surge-type flow: Journal of Geophysical Research, v. 92, p. 2883–2900.

Hay, A.E., Murray, J.W., and Burling, R.W., 1983, Submarine channels in Rubert Inlet, British Columbia: I, Morphology: Sedimentary Geology, v. 36, p. 289–315, doi: 10.1016/0037-0738(83)90013-1.

Hiscott, R.N., Hall, F.R., and Pirmez, C., 1997, Turbidity current overspill from Amazon Channel: Texture of the silt/sand load, paleoflow from anisotropy of magnetic susceptibility, and implications for flow processes, *in* Peterson, L.C., Proceedings of the Ocean Drilling Program, Scientific results, Volume 155: College Station, Texas, Ocean Drilling Program, p. 53–78.

Hungr, O., Morgan, G.C., and Kellerhals, R., 1984, Quantitative analysis of debris torrent hazards for design of remedial measures: Canadian Geotechnical Journal, v. 7, p. 221–238.

Imran, J., Parker, G., and Pirmez, C., 1999, A nonlinear model of flow in meandering submarine and subaerial channels: Journal of Fluid Mechanics, v. 400, p. 295–331, doi: 10.1017/S0022112099006515.

Imran, J., Parker, G., and Harff, P., 2002, Experiments on incipient channelization of submarine fans: Journal of Hydraulic Research, v. 40, p. 21–32.

Imran, J., Islam, M.A., Huang, H., Kassem, A., Dickerson, J., Pirmez, C., and Parker, G., 2007, Helical flow couplets in submarine gravity underflows: Geology, v. 35, p. 659–662, doi: 10.1130/G23780A.1.

Johannesson, H., and Parker, G., 1989, Secondary flow in mildly sinuous channel: Journal of Hydraulic Engineering, v. 115, p. 289–308.

Kassem, A., and Imran, J., 2005, Three-dimensional modeling of density current. II. Flow in sinuous confined and unconfined channels: Journal of Hydraulic Research, v. 42, p. 591–602.

Keevil, G.M., Peakall, J., Best, J.L., and Amos, K.J., 2006, Flow structure in sinuous submarine channels: Velocity and turbulence structure of an experimental submarine channel: Marine Geology, v. 229, p. 241–257, doi: 10.1016/j.margeo.2006.03.010.

Khripounoff, A., Vangriesheim, A., Babonneau, N., Crassous, P., Dennielou, B., and Savoye, B., 2003, Direct observations of intense turbidity current activity in the Zaire submarine valley at 4000 m water depth: Marine Geology, v. 194, p. 151–158, doi: 10.1016/S0025-3227(02)00677-1.

Kirkgoz, M.S., 1983, Breaking and run-up of long waves, *in* Iwasaki, T., ed., Tsunamis—Their science and engineering: Toyko, Terra Scientific, p. 467–478.

Kneller, B., 2003, The influence of flow parameters on turbidite slope channel architecture: Marine and Petroleum Geology, v. 20, p. 901–910, doi: 10.1016/j.marpetgeo.2003.03.001.

Komar, P.D., 1969, The channelized flow of turbidity currents with application to Monterey Deep-Sea Channel: Journal of Geophysical Research, v. 71, p. 4544–4558.

Langbein, W., and Leopold, L., 1966, River meanders and the theory of minimum variance, *in* Dury, G.H., ed., Rivers and river terraces, p. 238–263.

Lee, S.E., Talling, P.J., Ernst, G.G., and Hogg, A.J., 2002, Occurrence and origin of submarine plunge pools at the base of the U.S. continental slope: Marine Geology, v. 185, p. 363–377, doi: 10.1016/S0025-3227(01)00298-5.

Leopold, L.B., and Wolman, M.G., 1960, River meanders: Geological Society of America Bulletin, v. 71, p. 769–793.

Lien, T., Walker, R.G., and Martinsen, O.J., 2003, Turbidites in the Upper Carboniferous Ross Formation, western Ireland: Reconstructions of a channel and spillover system: Sedimentology, v. 50, p. 113–148, doi: 10.1046/j.1365-3091.2003.00541.x.

Makaske, B., and Weerts, H.J.T., 2005, Muddy lateral accretion and low stream power in the sub-recent confined channel belt, Rhine-Meuse delta, central Netherlands: Sedimentology, v. 52, p. 651–668, doi: 10.1111/j.1365-3091.2005.00713.x.

Middleton, G., 1993, Sediment deposition from turbidity currents: Annual Reviews in Earth and Planetary Sciences, v. 21, p. 89–114, doi: 10.1146/annurev.ea.21.050193.000513.

Mohrig, D., and Buttles, J., 2007, Shallow channels constructed by deep turbidity currents: Geology, v. 35, p. 155–158, doi: 10.1130/G22716A.1.

Mohrig, D., Straub, K.M., Buttles, J., and Pirmez, C., 2005, Controls on geometry and composition of a levee built

by turbidity currents in a straight laboratory channel, *in* Garcia, M.H., ed., River, coastal, and estuarine morphodynamics: RCEM 2005: London, Taylor and Francis Group, p. 579–584.

Morris, W., and Busby-Spera, C., 1990, A submarine-fan valley-levee complex in the Upper Cretaceous Rosario Formation: Implication for turbidite facies models: Geological Society of America Bulletin, v. 102, p. 900–914, doi: 10.1130/0016-7606(1990)102<0900: ASFVLC>2.3.CO;2.

Nanson, G.C., and Page, K.J., 1983, Lateral accretion of fine-grained concave benches on meandering rivers, *in* Lewin, J., ed., Modern and ancient fluvial systems: International Association of Sedimentologists Special Publication 6, p. 133–143.

Nelson, J.M., and Smith, J.D., 1989, Flow meandering channels with natural topography, *in* Parker, G., ed., River meandering: American Geophysical Union Water Resources Monograph 12, p. 69–101.

Nino, Y., Lopez, F., and Garcia, M.H., 2003, Threshold for particle entrainment into suspension: Sedimentology, v. 50, p. 247–263, doi: 10.1046/j.1365-3091.2003.00551.x.

Parker, G., Garcia, M.H., Fukushima, Y., and Yu, W., 1987, Experiments on turbidity currents over an erodible bed: Journal of Hydraulic Research, v. 25, p. 123–147.

Parsons, J.D., and García, M.H., 1998, Similarity of gravity current fronts: Physics of Fluids, v. 10, p. 3209–3213, doi: 10.1063/1.869848.

Peakall, J., McCaffrey, B., and Kneller, B., 2000, A process model for the evolution, morphology, and architecture of sinuous submarine channels: Journal of Sedimentary Research, v. 70, p. 434–448.

Piper, D.J.W., and Normark, W.R., 1983, Turbidite depositional patterns and flow characteristics, Navy submarine fan, California Borderland: Sedimentology, v. 30, p. 681–694, doi: 10.1111/j.1365-3091.1983.tb00702.x.

Pirmez, C., 1994, Growth of a submarine meandering channel-levee system on the Amazon Fan [Ph.D. thesis]: New York, Columbia University, 587 p.

Pirmez, C., and Imran, J., 2003, Reconstruction of turbidity currents in Amazon Channel: Marine and Petroleum Geology, v. 20, p. 823–849, doi: 10.1016/j.marpetgeo.2003.03.005.

Pirmez, C., and Flood, R.D., 1995, Morphology and structure of Amazon channel, *in* Peterson, L.C., Proceedings of the Ocean Drilling Program, Initial results, Volume 155: College Station, Texas, Ocean Drilling Program, p. 23–45.

Pirmez, C., Hiscott, R.N., and Kronen, J.D., 1997, Sandy turbidite successions at the base of channel-levee systems of the Amazon fan revealed by FMS logs and cores: Unraveling the facies architecture of large submarine fans, *in* Peterson, L.C., Proceedings of the Ocean Drilling Program, Scientific results, Volume 155: College Station, Texas, Ocean Drilling Program, p. 7–33.

Pirmez, C., Beaubouef, R.T., Friedmann, S.J., and Mohrig, D., 2000, Equilibrium profile and baselevel in submarine channels: Examples from late Pleistocene systems and implications for the architecture of deepwater reservoirs, *in* Weimer, P., et al., eds., Deep-water reservoirs of the world: GCSEPM Foundation 20th Annual Bob F. Perkins Research Conference, p. 782–805.

Posamentier, H.W., 2003, Depositional elements associated with a basin floor channel-levee system: Case study from the Gulf of Mexico: Marine and Petroleum Geology, v. 20, p. 677–690, doi: 10.1016/j.marpetgeo.2003.01.002.

Posamentier, H.W., and Kolla, V.E., 2003, Seismic geomorphology and stratigraphy of depositional elements in deep-water settings: Journal of Sedimentary Research, v. 73, p. 367–388.

Posamentier, H.W., Meizarwin, P.S., Wisman, T., and Plawman, 2000, Deep water depositional systems—Ultra deep Makassar Strait, Indonesia, *in* Weimer, P., et al., eds., Deep-water reservoirs of the world: GCSEPM Foundation 20th Annual Bob F. Perkins Research Conference, p. 806–816.

Prior, D.B., Bornhold, B.D., Wiseman, J.W.R., and Lowe, D.R., 1987, Turbidity current activity in a British Columbia fjord: Science, v. 237, p. 1330–1333, doi: 10.1126/science.237.4820.1330.

Rozovskii, I.L., 1961, Flow of water in bends of open channels: Washington, D.C., Office of Technical Service, US Department of Commerce, No. OTS 60–51133.

Rubin, D.M., and Hunter, R.E., 1982, Bedform climbing in theory and nature: Sedimentology, v. 29, p. 121–138, doi: 10.1111/j.1365-3091.1982.tb01714.x.

Schmidt, J.C., Rubin, D.M., and Ikeda, H., 1993, Flume simulation of recirculating flow and sedimentation: Water Resources Research, v. 29, p. 2925–2939, doi: 10.1029/93WR00770.

Shor, A.N., Piper, D.J.W., Clarke, J.E., and Mayer, L.A., 1990, Giant flute-like scour and other erosional features formed by the 1929 Grand Banks turbidity current: Sedimentology, v. 37, p. 631–645, doi: 10.1111/j.1365-3091.1990.tb00626.x.

Skene, K.I., 1998, Architecture of submarine channel levees [Ph.D. thesis]: Halifax, Nova Scotia, Canada, Dalhousie University, 365 p.

Skene, K.I., Piper, D.J.W., and Hill, P.S., 2002, Quantitative analysis of variations in depositional sequence thickness from submarine channel levees: Sedimentology, v. 49, p. 1411–1430, doi: 10.1046/j.1365-3091.2002.00506.x.

Smith, J.D., and McLean, S.R., 1984, A model for flow in meandering streams: Water Resources Research, v. 20, p. 1301–1315.

Starn, R.H., 1981, Light attenuation in natural waters: Gershun's law, Lambert-Beer law, and the mean light path: Applied Optics, v. 20, p. 2326–2338.

Stelting, C.W., Pickering, K., Bouma, A., Coleman, J.M., Cremer, M., Droz, L., Meyer-Wright, A.A., Normark, W.R., O'Connell, S., Stow, D.A., and Scientist, D.L.S., 1985, Drilling results on the Middle Mississippi Fan, *in* Normark, W.R., ed., Submarine fans and related turbidite sequences: New York, Springer-Verlag, p. 275–282.

Xu, J.P., Nobel, M.A., and Rosenfeld, L.K., 2004, In-situ measurements of velocity structure within turbidity currents: Geophysical Research Letters, v. 31, doi: 10.1029/2004GL019718.

Yen, C., and Yen, B.C., 1971, Water surface configuration in channel bends: Journal of Hydraulic Engineering, v. 97, p. 303–321.